Department of Communications and Networking

On Performance of Limited Feedback Coordinated Multipoint Transmission for Mobile Systems

Beneyam Berehanu Haile

Aalto University

DOCTORAL DISSERTATIONS

Aalto University publication series
DOCTORAL DISSERTATIONS 129/2016

On Performance of Limited Feedback Coordinated Multipoint Transmission for Mobile Systems

Beneyam Berehanu Haile

A doctoral dissertation completed for the degree of Doctor of Science (Technology) to be defended, with the permission of the Aalto University School of Electrical Engineering, at a public examination held at the lecture hall S1 of the school on 25th of August 2016 at 12:00 (at noon).

Aalto University
School of Electrical Engineering
Department of Communications and Networking

Supervising professor
Prof. Jyri Hämäläinen (Aalto University, Finland)

Thesis advisor
Dr. Edward Mutafungwa (Aalto University, Finland)

Preliminary examiners
Prof. Mohammed Elmusrati (University of Vaasa, Finland)
Prof. Ana I. Perez-Neira (Centre Tecnològic de Telecomunicacions de Catalunya, Spain)

Opponents
Prof. Mikko Valkama (Tampere University of Technology, Finland)
Prof. Mohammed Elmusrati (University of Vaasa, Finland)

Aalto University publication series
DOCTORAL DISSERTATIONS 129/2016

ISBN 978-952-60-6895-4 (printed)
ISBN 978-952-60-6896-1 (pdf)
ISSN-L 1799-4934
ISSN 1799-4934 (printed)
ISSN 1799-4942 (pdf)
http://urn.fi/URN:ISBN:978-952-60-6896-1

Unigrafia Oy
Helsinki 2016

Finland

441 697
Printed matter

Aalto University

Abstract

Aalto University, P.O. Box 11000, FI-00076 Aalto www.aalto.fi

Author
Beneyam Berehanu Haile

Name of the doctoral dissertation
On Performance of Limited Feedback Coordinated Multipoint Transmission for Mobile Systems

Publisher School of Electrical Engineering

Unit Department of Communications and Networking

Series Aalto University publication series DOCTORAL DISSERTATIONS 129/2016

Field of research Communication Engineering

Manuscript submitted 2 March 2016 **Date of the defence** 25 August 2016

Permission to publish granted (date) 23 May 2016 **Language** English

☐ **Monograph** ☒ **Article dissertation** ☐ **Essay dissertation**

Abstract

Mobile networks are expected provide consistent quality of experience across the service area. Yet, intercell interference is one of the main causes for the inconsistent user experience in contemporary mobile systems especially when the universal reuse of spectrum is applied. To mitigate and/or even exploit the intercell interference, coordinated multipoint (CoMP) transmission/reception has been considered as a promising technique and it is incorporated in the fourth generation mobile standard. Various CoMP techniques have been investigated in literature and practice, each offering differing trade-offs between performance and implementation requirements. Thus, effective use of various CoMP realizations requires thorough understanding of the mentioned trade-offs associated with each CoMP technique.

The contribution of this thesis includes practical approaches for development of effective CoMP transmission methods. Dissertation investigates the methods from three perspectives, namely: by proposing a flexible and practical hierarchical feedback structure to effectively combine different beamforming techniques in CoMP transmission; by studying the performance degradation of CoMP systems due to channel power imbalance in practical CoMP methods with limited feedback; and by evaluating CoMP performance gains in realistic urban deployment scenarios using deterministic 3D propagation models.

Performance results reveal that in addition to implementation flexibility, notable performance gain can be achieved by simple limited feedback CoMP methods. Our results also demonstrate that the use of amplitude feedback – fast or slow – is important to effectively compensate the impact of channel power imbalance. Furthermore, our results show that CoMP may significantly relax the capacity gap between backhaul and access links of self-backhauled low power nodes.

Keywords User Experience, Intercell Interference, Coordinated Multipoint, Hierarchical Beamforming, Channel Power Imbalance, Self-backhauling, Low Power Nodes, QoE, 4.5G, CoMP, Relay, Smallcell

ISBN (printed) 978-952-60-6895-4 **ISBN (pdf)** 978-952-60-6896-1

ISSN-L 1799-4934 **ISSN (printed)** 1799-4934 **ISSN (pdf)** 1799-4942

Location of publisher Helsinki **Location of printing** Helsinki **Year** 2016

Pages 195 **urn** http://urn.fi/URN:ISBN:978-952-60-6896-1

Preface

መኑ ከመ እግዚአብሔር!

The research work for this doctoral thesis has been carried out at the Department of Communications and Networking (COMNET) of Aalto University School of Electrical Engineering, Espoo, Finland during 2011-2016. This work was funded by Academy of Finland, Finnish Funding Agency for Technology and Innovation, European Institute of Innovation and Technology, and National Science Foundation.

First of all, I would like to express my utmost gratitude to my supervisor Prof. Jyri Hämäläinen for his continuous encouragement, support, enlightening discussions and, mainly, for providing me this opportunity. It has been a pleasure and a great honor to work with him. I would also like to sincerely thank my advisor Dr. Edward Mutafunguwa who has provided me with the necessary support and guidance at all phases of this work.

Special thanks to Prof. Zhi Ding for his hospitality and encouragement during my research visit to Department of Electrical and Computer Engineering, University of California, Davis. I would also like to thank my co-author Dr. Alexis A. Dowhuszko for the help and thoughtful discussions.

I would like to thank the thesis pre-examiners Prof. Mohammed Elmusrati and Prof. Ana I. Perez-Neira for their valuable comments and suggestions. I would also like to thank Prof. Mikko Valkama and Prof. Mohammed Elmusrati for accepting to be the defense opponent. I am grateful to Prof. Heikki Hämmäinen for being in charge of my supplementary field.

I would like to thank my colleagues at School of Electrical Engineering for the good time and encouragement, including Emma Jokinen, Dr.

Zhong Zheng and Dr. David Gonzalez. I also acknowledge the COMNET operating engineer Viktor Nässi and all the support personnels for their continuous practical guidance.

I would like to take this opportunity to pay my gratitude to people who are close to me for their unique support during both the high and low times: Yihenew Beyene, Alem Tsehay (and her family), Nebi Atsedemariam, Tenager Bekalu, Merkebu Zenebe, Yonas Abebe, Ezana Zerihune and all the wonderful people at EOTC Helsinki and Ethio-Fin sport club.

My special intimate thanks go to my extraordinary mother, Yeshumnesh Zergaw, strong father, Birhanu Haile and all lovely siblings for the love and encouragement they have given me over the years. My deepest gratitude also goes to my love, Melkam Kibur who constantly brings joy and happiness to my life.

Espoo, June 21, 2016,

Beneyam B. Haile

Contents

List of Publications

This thesis consists of an overview and of the following publications which are referred to in the text by their Roman numerals.

I B. B. Haile and J. Hämäläinen. Performance analysis of hierarchically combined practical beamforming methods. *Wireless Personal Communications* , vol. 84, no. 3, pp. 1855-1875, April 2015.

II B. B. Haile, A. Dowhuszko, J. Hämäläinen, R. Wichman and Z. Ding. On performance loss of some CoMP techniques under channel power imbalance and limited feedback. *IEEE Transactions on Wireless Communications* , vol. 14, no. 8, pp. 4469-4481, August 2015.

III B. B. Haile, J. Hämäläinen and Z. Ding. Power imbalance induced BER performance loss under limited feedback CoMP techniques. *submitted to EURASIP Journal on Communications and Networking* , vol. xx, no. xx, pp. xx-x, xx 2016.

IV B. B. Haile, E. Mutafungwa and J. Hämäläinen. Coordinated multipoint transmission for LTE-Advanced networks in dense informal settlements. In *IEEE AFRICON 2013*, Pointe-Aux-Piments, pp. 1-5, September 2013.

V B. B. Haile, E. Mutafungwa and J. Hämäläinen. Coordinated multipoint transmission for relaxation of self-backhauling bottlenecks in heterogeneous networks. *EURASIP Journal on Wireless Communications and Networking*, vol. 2015, no. 1, March 2015.

VI B. B. Haile, E. Mutafungwa and J. Hämäläinen. Use of coordinated multipoint transmission for relaxation of relay link bottlenecks. In *IEEE 79th Vehicular Technology Conference Spring (VTC-Spring 2014)*, Seoul, pp. 1-5, May 2014.

VII B. B. Haile, E. Mutafungwa and J. Hämäläinen. LTE-Advanced enhancements for self-backhauled LTE-U small cells: An addis ababa case study. In *IEEE AFRICON 2015*, Addis Ababa, pp. 1-5, September 2015.

Author's Contribution

Publication I: "Performance analysis of hierarchically combined practical beamforming methods"

The author of this thesis had the lead role in this paper. The techniques provided in this paper have been developed in cooperation between the authors. Furthermore, the author of this thesis has deduced the analytical formulae, analyzed the techniques and written the paper.

Publication II: "On performance loss of some CoMP techniques under channel power imbalance and limited feedback"

The author of this thesis had the lead role in this paper. The general framework of this work has been developed in cooperation among the authors. The author of this thesis has deduced the closed-form expressions, analyzed the techniques provided in the paper and written the paper.

Publication III: "Power imbalance induced BER performance loss under limited feedback CoMP techniques"

The author had the main responsibility for deriving the analytical expressions, analyzing the techniques and writing this article.

Publication IV: "Coordinated multipoint transmission for LTE-Advanced networks in dense informal settlements"

The author had the main responsibility in developing and analyzing the methods provided in this paper. The author has carried out the system-

level simulations and written the paper.

Publication V: "Coordinated multipoint transmission for relaxation of self-backhauling bottlenecks in heterogeneous networks"

The author of this thesis had the lead role in developing and analyzing the techniques provided in the paper and writing the paper. The author has carried out the theoretical analysis and the system-level simulations.

Publication VI: "Use of coordinated multipoint transmission for relaxation of relay link bottlenecks"

The author of this thesis had the lead role in developing and analyzing the techniques provided in this paper. The author of this thesis has carried out the system-level simulations and written the paper.

Publication VII: "LTE-Advanced enhancements for self-backhauled LTE-U small cells: An addis ababa case study"

The author had the main responsibility for formulating the techniques, performing the system-level simulations and writing this article.

List of abbreviations and symbols

Abbreviations

3GPP	3rd generation partnership project
5G	fifth generation
AWGN	additive white Gaussian noise
BER	bit error rate
BS	base Station
CC	quantized co-phasing-quantized co-phasing
CCL	quantized co-phasing-quantized co-phasing with large feedback bits
CDF	cumulative distribution function
CoMP	coordinated multipoint
CS	quantized co-phasing-selection
CSI	channel State Information
DAS	distributed antenna system
e2e	end-to-end
eNB	evolved NodeB
FDD	frequency division duplexing
FI	full CSI
HSPA	high speed packet access
ICI	intercell interference
JP	joint processing
LOS	line-of-sight
LPN	low-power node
LTE	long term evolution
LTE-A	long term evolution-advanced
LTE-U	long term evolution in unlicensed spectrum
MIMO	multiple-input multiple-output

MS	mobile station
OQCP	ordered quantized co-phasing
PRB	physical resource block
QCP	quantized co-phasing
QoE	quality of experience
RAN	radio access network
RN	relay node
RR	round robin
SINR	signal-to-noise-plus-interference ratio
SNR	signal-to-noise ratio
SC	selection-quantized co-phasing
SS	selection-selection
TSC	transmit selection combining
UE	user equipment
WCDMA	wideband code division multiple access

Symbols

$\|\cdot\|$	Euclidean norm
B_{eff}	bandwidth efficiency
B_{PRB}	bandwidth per PRB
C	capacity of a system of interest
$\mathbb{E}\{\cdot\}$	expectation
$\mathcal{F}$	fading figure
$f(\cdot)$	probability distribution function
$\mathcal{G}$	expected value of instantaneous SNR
$\mathbf{g}$	signal vector
g_m	signal coefficient at m^{th} antenna group
$\mathbf{h}_m$	channel gain vector of m^{th} antenna group
$h_{m,k}$	channel gain at k^{th} antenna of m^{th} antenna group
K	Rician factor
L	number of antenna group
M	number of antennas
N_{PRB}	number of PRB
N	number of feedback bits for selection of phase weight
n	zero-mean complex additive white Gaussian noise
P_e	average bit error rate
P_n	noise power
P_o	outage probability
P_t	total transmitted energy per channel use
Q	CoMP set
$\mathcal{Q}$	number of BS in CoMP set Q
r	received signal
$\mathcal{S}$	spectral efficiency
s	information symbol
T	target threshold
$\mathcal{T}$	throughput
$\mathbf{u}_m$	complex weight vector for m^{th} antenna group
u	BS transmit power factor
$u_{m,k}$	transmit weight at k^{th} antenna of m^{th} antenna group
v_m	amplitude weight at m^{th} antenna group
$\mathbf{w}$	complex weight vector for coordination
w_m	transmit weight at m^{th} antenna group
$\mathbf{x}_m$	transmitted vector signal from m^{th} antenna group

Z_r	required SINR
z	instantaneous SNR
z_{eff}	SINR efficiency
γ_m	signal power at m^{th} antenna group
$\gamma_{m,k}$	channel power at k^{th} antenna of m^{th} antenna group
$\gamma_{(1)}$	maximum of γ_1 and γ_2
$\gamma_{(2)}$	minimum of γ_1 and γ_2
$\bar{\gamma}$	average transmit SNR
$\bar{\gamma}_m$	expected value of channel power of an antenna from m^{th} group
θ	residual phase difference
σ_0	channel power imbalance
τ_r	time share for relay link
ϕ_m	phase weight at m^{th} antenna group
ψ_m	signal phase at m^{th} antenna group
$\psi_{m,k}$	channel phase at k^{th} antenna of m^{th} antenna group

1. Introduction

1.1 Background and motivation

Mobile communications has become a pervasive and essential part of everyday life in modern society providing diverse voice and data services for over 7.4 billion subscribers globally [1]. The adoption of various mobile data services and applications has contributed to significant growth in mobile data traffic. A key driver is the increased penetration of powerful mobile devices with ever growing storage capacity and default features, such as, high resolution cameras. In 2014, for instance, the volume of mobile data traffic was roughly 30 times the size of the entire global Internet in 2000 and it is predicted to rise almost tenfold between 2014 and 2019 [1]. Besides, accommodating the increasing traffic, mobile operators and their networks are expected to consistently meet (and exceed) end user expectation for sufficiently high data rate and acceptable quality of experience (QoE) levels regardless of user location and time.

How can we increase network capacity and achievable data rate? What comes to the single-antenna point-to-point link performance, it has been noted that we cannot achieve any significant improvement as current mobile systems have already approached the theoretical Shannon capacity. Even long term evolution (LTE) Release 8 is performing less than 2 dB off the theoretical limit [2]. A number of other options are available for boosting data rate, this includes, providing additional spectrum, increasing the number of antennas and having a denser deployment of base stations (BSs) [3]. Data rate increases linearly with bandwidth and more bandwidth can be obtained by aggregating fragmented spectrum. In LTE-Advanced (LTE-A), carrier aggregation has extended the 20 MHz basic LTE bandwidth upto 100 MHz, and the future fifth generation (5G)

network is also exploring the possibility of using a broad range of spectrum bands available above 6 GHz while efficiently reusing existing bands below 6 GHz [4]. Furthermore, applying n additional transmit and receive antennas for the same bandwidth ideally provides $n-$fold data rate through data multiplexing, and LTE-A supports 8-layer downlink transmission extending the 4-layer transmission of LTE Release 8/9 [3]. Massive antenna usage for further data rate improvement are also being considered for 5G [5]. Moreover, high data rate can also be achieved by reducing user-to-BS distance with densification of BSs where low-power nodes (LPNs) (such as small cells and relay nodes (RNs) incorporated in LTE-A) are introduced under the conventional macro deployment [3]. Ultra dense networks are also being considered for 5G [6].

Do the above data rate enhancement methods guarantee homogeneous QoE across serving area of mobile networks? The answer is 'no' as neither of them directly address intercell interference (ICI) that is the main cause of inconsistent user experience in modern cellular systems that are designed to reuse the whole available spectrum in all cells. Due the presence of ICI, significant percentage of cell-edge users experience much lower throughput than cell-center users [7]. The densification of BS expands the fraction of cell-edge area where the multilayer transmission is almost impossible because of low signal-to-interference-plus-noise ratio (SINR).

To mitigate and/or exploit ICI for improved homogeneity of QoE, dynamic coordination of neighbouring BSs has been considered under the name coordinated multipoint (CoMP) transmission/reception. CoMP has been vastly studied [8–12] while practical CoMP techniques have been incorporated in LTE-A since Release 11 [13, 14]. In 3^{rd} generation partnership project (3GPP), CoMP transmission refers to the so-called joint processing (JP) and coordinated scheduling/beamforming [13–15]. In JP CoMP, transmitted data to a single user is available at each transmission point of a CoMP set while, in coordinated beamforming/scheduling, transmission is executed from one BS but user beamforming/scheduling decisions are coordinated to mitigate ICI.

Various codebooks for CoMP transmission exhibit different performance benefits and different requirements on feedbacking, backhauling, clustering, synchronization, and other implementation factors [9, 16, 17]. Various tradeoffs have been noted between benefits of CoMP algorithms and their implementation requirements. Thus, it is important to explore the tradeoff among performance, complexity and cost in order to effectively apply

the CoMP methods.

1.2 Objectives, scope and research problems

This thesis has three main objectives. The first objective is to introduce, model, and analyse a hierarchical feedback structure that enables flexible combination of the different beamforming methods for CoMP transmission in frequency division duplexing (FDD) downlink system. Unless explicitly mentioned, CoMP in this thesis refers the downlink CoMP transmission.

Since the spatially distributed transmissions in CoMP can lead to mean channel power imbalance at reception, the second objective of the thesis is to thoroughly investigate the tradeoff between channel power imbalance and performance benefits of CoMP.

In the investigation of both hierarchical feedback and impact of channel power imbalance, analysis for some extended versions of 3GPP feedback techniques has been made. In both cases, it is very difficult to attain distribution for received signal-to-noise ratio (SNR) that could be used to derive analytical results for performance gains and losses. Hence, related to first two objectives, the thesis addresses the following questions on the performance analysis:

- How to develop analytical tools for important performance metrics by which we can quantify and analyze coherent combining and diversity gains for hierarchical feedback methods for CoMP?

- How to derive analytical formulas by which we can quantify and analyze performance losses incurred by channel power imbalance in CoMP transmission?

- How to provide insights on performance gains and losses for the different feedback techniques of CoMP using the developed analytical tools?

Finally, we note that most of system simulations carried out for CoMP have considered uniform network layouts and empirical propagation models [13, 14]. The third main objective is to evaluate CoMP applied in LTE networks deployed in exemplary urban scenarios considering deterministic 3D propagation models. This study focus on the CoMP performance

while applied to resolve the backahul capacity bottleneck challenge of self-backhauled LPNs in heterogeneous deployment. Thus, through simulation campaigns, the following important questions are addressed:

- How practical CoMP methods perform in realistic deployment scenario?
- How far CoMP can be used to relax the backahul capacity bottleneck of self-backahuled LPNs in heterogeneous network deployment?

1.3 Contributions and summary of publications

The thesis first introduces hierarchical feedback structure for CoMP transmission and undertakes mathematical analysis of the proposed hierarchical system when combining two practical low-rate feedback methods: the so-called quantized co-phasing (QCP) that exploits channel phase information and is a straightforward extension of feedback technique standardized in wideband code division multiple access (WCDMA)/high speed packet access (HSPA) and LTE systems, and the classical transmit selection combining (TSC). Closed-form expressions for expected SNR, fading figure and average bit error rate (BER) are formulated [PI]. While the expected SNR provides insight on the benefit obtained from the coherent combining, the fading figure and the average BER quantify achieved diversity gain.

The thesis also provides thorough analysis on performance degradation due to channel power imbalance for the low-rate feedback methods [PII and PIII]. Besides QCP and TSC, the analysis has also been carried out for ordered QCP (OQCP) method that exploits channel amplitude information on top of the channel phase information. To investigate impact of channel power imbalance, analytical expressions for optimal amplitude weights, expected SNR, asymptotic capacity and BER are developed [PII and PIII]. While expected SNR and asymptotic capacity provide insight into the impact of channel power imbalance on the benefit of coherent combining, asymptotic BER presents power imbalance impact on the diversity gain.

For benchmarking, analytical results are provided for the case where full phase and/or channel state information (CSI) is available at the transmitter side. Derived analytical results are all verified numerically. Fur-

thermore, detailed performance experiments are performed to observe performance losses due to channel power imbalance for the various CoMP methods. Finally, impact of feedback bit errors is highlighted using numerical analysis [PII and PIII].

Through system-level simulations, the thesis evaluates spectral efficiency and throughput gains that are achievable with QCP based CoMP applied in LTE networks deployed in exemplary dense urban areas of Tanzania and Ethiopia [PIV-PVII]. Propagation is computed deterministically using dominant path model based on realistic 3D building and terrain maps and 3D antenna pattern. The evaluation is mainly focused on the use of CoMP in the wireless backhaul of self-backhauled LPN assuming LTE-A relay backhaul link [PV and PVI] and, on the other hand, LTE in unlicensed spectrum (LTE-U) [PVII]. Insights on possible performance degradations due to different levels of feedback errors for QCP method are also provided.

Besides the simulation based evaluations, an analytical expression for outage probability is presented for QCP based CoMP technique considering Rician fading channel towards the serving BS and Rayleigh fading channels towards the adjacent BSs [PV]. The Rician fading channel towards the serving BS is based on the assumption that LPNs have line-of-sight (LOS) connection from their serving BS, which is mostly the case for outdoor LPNs deployed at rooftop level.

1.4 Structure of thesis

The rest of the thesis is structured as follows.

Chapter 2 first provides a brief background on the CoMP techniques. Then the chapter presents overview of the hierarchical feedback structure and the 3GPP feedback techniques. Also definitions of the used performance metrics are provided.

Chapter 3 summarizes analytical results obtained when assuming the hierarchical feedback structure. The results summarized in this chapter are obtained for different combinations of QCP and TSC beamforming techniques. Expected SNR, fading figure, and average BER metrics are considered in the performance analysis.

Chapter 4 presents analytical results quantifying channel power imbalance impact on CoMP transmission and performance discussion based on the results. The performance measure is based on expected SNR, asymptotic capacity and BER.

Chapter 5 provides performance evaluation of CoMP when applied in realistic LTE urban deployments, particularly to relax backhaul capacity bottleneck of LPNs. LTE-A relay and LTE-U concepts are considered in the evaluation.

Chapter 6 is the final chapter providing concluding remarks and implications. Prospects on potential future research items are also outlined in this chapter.

2. Coordinated multipoint transmission

2.1 Background of CoMP techniques

CoMP methods provide means for coordination of transmissions from multiple BSs to address intercell interference resulting inconsistent user experience [18]. The coordination in CoMP is dynamic in contrast to the semi-static coordination in the soft frequency reuse and the so-called enhanced intercell interference coordination [19]. In the conventional mobile network deployment, the coordination takes place among neighbouring cells operated at same site (intra-site CoMP) or/and at different sites (inter-site/inter-tier CoMP). The level of coordination among cells can extend from basic information exchange for considerate scheduling/beamforming decisions of BSs to complex JP where BSs together transmit same message to CoMP user [10]. It is important to note that JP CoMP is suited to more centralized architectures (such as distributed antenna system (DAS) [20]) where transmission is done from geographically distributed antennas while base band processing is centralized.

Several theoretical studies have been carried out to design and analyze various optimal and suboptimal CoMP techniques [8, 11, 12, 21, 22]. CoMP algorithms maximizing weighted sum rate are discussed in [21, 22] while authors in [11] and [12] develop and analyze algorithms providing optimal beamformers across all coordinating BSs to minimize total transmitted power [11] and backhaul capacity demand [12]. In FDD system, CoMP methods assuming perfect CSI at BSs are not practical because of unrealistic feedback overheads. In this case, we consider low-rate optimal and sub-optimal feedback methods [23] that have been proposed already when simple transmit diversity methods were introduced in the late 90s [24–26]. Literature has showed that the various CoMP algorithms

provide significant amount of gains in terms of spectral efficiency that can be exploited to provide homogeneous user experience across mobile networks. For this reason, CoMP has been considered as an important technology in 3GPP LTE-A [27].

The performance benefits of various CoMP methods applied for LTE-A system have been illustrated by a number of simulation campaigns and field trails considering different deployment scenarios [9, 10, 14, 15, 18, 28]. For instance, simulations in [15] and [10] for specific scenarios showed that JP CoMP provides 58% and 92% cell-edge UE throughput gains over non-CoMP. The technical reports in [14, 28] also presented various amounts of CoMP gains in terms of cell-edge UE and average cell throughputs identified by members of 3GPP considering various CoMP algorithms. These performance benefits of CoMP have been validated through field trials presented in [9, 10, 29].

However, practical implementation of JP CoMP face challenges in terms of capacity and reliability of feedback and backhaul systems, clustering policy and synchronization techniques [9, 17]. Note that coordinating BSs share not only user data and scheduling information but also CSI, and in principle, the more accurate the CSI feedback the better the CoMP performance. In other words, limited feedback capacity and feedback errors/delays degrade CoMP performance the tradeoffs being detailed in [9, 28–34]. These capacity and reliability challenges in case of inter-site CoMP extend to the backhaul between coordinating BSs since the information needs to be exchanged among the BSs located at different sites [12, 14, 35]. This backhaul challenge leads us also to clustering problem where we need efficient definition of the coordination area in order to achieve good performance and manageable backhaul overheads [36]. Furthermore, coordinating BSs need to be synchronized in time and frequency to successfully avoid intersymbol and intercarrier interference; this is possible today but size of the geographical coordination area is limited by length of the cyclic prefix in orthogonal frequency-division multiple access systems [17].

It has been noted that some of the backhaul challenges can be better addressed in potential 5G radio access network (RAN) architectures such as cloud-RAN making CoMP more applicable [29, 37]. Furthermore, the backhaul overhead associated with JP CoMP can also be reduced by applying complementary massive multiple-input multiple-output (MIMO) [5]. Yet, we note at this point that different feedback

methods for CoMP present different performance gains with different implementation challenges [16]. Therefore, to bring additional flexibility on the use of the different CoMP schemes with less strict implementation requirements, this thesis introduce a hierarchical feedback structure [PI].

2.2 Hierarchical feedback structure and system model

2.2.1 Hierarchical feedback structure

The hierarchical structure for CoMP is depicted in Figure 2.1 where co-located or distributed transmit antennas are organized into L groups of M antennas. Within grouping appropriate precoding methods are selected for each antenna group and for coordination between the groups to achieve reliable transmission towards the mobile station (MS) receiver. The receiver sends two levels of feedback to select the precoding weights. Namely, the feedback to different groups of antennas and the feedback for adjusting sum signals from antenna groups.

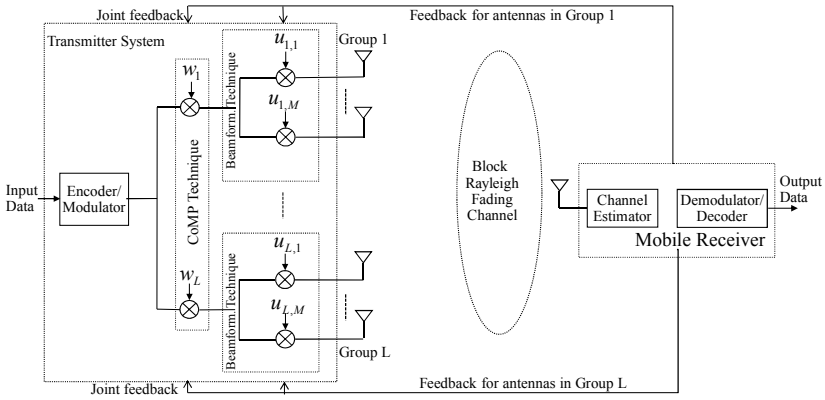

Figure 2.1. System model for CoMP transmission using hierarchical feedback structure.

Although the hierarchical structure can be applied in almost any multiple-input single-output system, this thesis focuses on the CoMP system where each group of antennas are located in the same BS site or different sites. It is important to note that the hierarchical structure provides at least the following benefits:

- Different kind of precoding methods can be used within antenna groups and over the groups. This capability provides us the flexibility to choose suitable precoding techniques taking into account various implementa-

tion challenges and requirements.

- If antenna groups are located at different BSs, then mobile terminal can easily provide antenna group specific feedback over separate control channels.
- In case of inter-site CoMP, hierarchical system produces less backhaul overhead than joint feedback that is based on the resultant signals from all groups.
- Overall sensitivity to feedback errors is reduced as system uses independent feedback words instead of fully joint feedback words.

The first of the aforementioned advantages can have practical value when, for example, antenna configurations are different in BSs that cooperate in transmission. Furthermore, if mean signal strengths of the BSs are different, then more accurate feedback can be provided for the strongest groups in adaptive feedback system.

2.2.2 Signal model

In the system model, the received signal at time instant i can be written in the form

$$r[i] = \sum_{m=1}^{L} \mathbf{h}_m \cdot \mathbf{x}_m[i] + n[i] = \sum_{m=1}^{L} [(\mathbf{h}_m \cdot \mathbf{u}_m)w_m]s[i] + n[i], \qquad (2.1)$$

where $\mathbf{x}_m[i] \in \mathbb{C}^{1\times M}$ is the transmitted vector signal from the m^{th} group of antennas containing the information symbol $s[i]$, $\mathbf{h}_m \in \mathbb{C}^{1\times M}$ is the channel gain vector of the m^{th} group, $n[i]$ refers to *zero-mean* complex additive white Gaussian noise (AWGN) with average power P_{n}, and the dot $'\cdot'$ refers to dot product. We note that $\mathbf{x}_m[i]$ results from $s[i]$ via beamforming, where $\mathbf{w} = (w_1, w_2, \ldots, w_L)$ and $\mathbf{u}_m$ with normalized powers $\|\mathbf{w}\| = 1$ and $\|\mathbf{u}_m\| = 1$ represent complex vectors with weights selected from respective codebooks. The power constraint for the input signal implies that $\sum_{m=1}^{L} \mathbb{E}\left\{\mathbf{x}_m \mathbf{x}_m^{\dagger}\right\} \leqslant P_{\text{t}}$, where P_{t} is the total transmitted energy per channel use and $(\cdot)^{\dagger}$ denotes Hermitian transpose. We do not consider fast power control mechanisms at the transmitter side. Therefore, P_{t} remains fixed for the duration of the data packet (frame) transmission.

We have assumed a flat block fading channel model such that channel gains remain constant during each block/frame of transmitted symbols, and channel responses of temporally separate transmission blocks are independent. The channel coefficients $h_{m,k} = \sqrt{\gamma_{m,k}}\, e^{j\psi_{m,k}}$ $(m = 1, 2, \ldots, L; k = 1, 2, \ldots, M)$ are described by zero-mean complex Gaussian

random variables. Thus, $\gamma_{m,k}$ follow exponential distribution and phases $\psi_{m,k}$ are uniformly distributed.

We let $g_m = \mathbf{h}_m \cdot \hat{\mathbf{u}}_m = \sum_{k=1}^{M} h_{m,k}\hat{u}_{m,k} = \sqrt{\gamma_m}e^{j\psi_m}$ denote the sum signal from m^{th} group with a selected weight vector $\hat{\mathbf{u}}_m$. Furthermore, for a selected weight vector $\hat{\mathbf{w}}$, the instantaneous SNR, denoted by z, can be written as

$$z = |\mathbf{g} \cdot \hat{\mathbf{w}}|^2, \tag{2.2}$$

where $\mathbf{g} = (g_1, g_2, \ldots, g_L)$. The studied limited feedback precoding algorithms to select the transmit weights are briefly discussed in the next section.

2.3 Limited feedback methods for CoMP

To determine the weight vectors $\hat{\mathbf{w}}$ for coordination and $\hat{\mathbf{u}}_m$ for antenna branches in the m^{th} group, we can apply various limited-feedback methods [23]. The performance analysis considers combinations of limited feedback methods that are extended versions of 3GPP transmit diversity techniques. To back up the discussion in the forthcoming sections, we briefly present the methods for the selection of $\hat{\mathbf{w}}$. The definitions can be applied simply for $\hat{\mathbf{u}}_m$ by replacing $\mathbf{g}$ and L with $\mathbf{h}_m$ and M, respectively.

2.3.1 Transmitter selection combining

This is a classical and simple method where codebook consist of L vectors of the form $\mathbf{w} = (0, \ldots, 0, 1, 0, \ldots, 0)$ such that the non-zero component indicates antenna group providing best SNR. In other words, the best weight $\hat{\mathbf{w}}$ is selected according to $|\mathbf{g} \cdot \hat{\mathbf{w}}| = \max\{\sqrt{\gamma_m} : m = 1, 2, \ldots, L\}$. The main benefit of TSC is its small $\lceil \log_2(L) \rceil$-bit feedback overhead which makes the method attractive from a practical implementation perspective. It has also been considered in the JP CoMP category of 3GPP under the name dynamic point selection [28]. However, the performance of TSC is inferior to more sophisticated feedback algorithms and it is also very sensitive to errors in feedback signaling [30, 31].

2.3.2 Quantized co–phasing

As the name tells, QCP adjusts relative phases between component signals. The MS assumes one of the received signals (e.g. one of the antenna

groups) as a reference (say the 1^{st} one). Then it independently selects phase weights ϕ_m for remaining antenna groups based on

$$\phi_m = \arg\max_{\phi} \left| g_1 + g_m e^{j\phi} \right|, \tag{2.3}$$

where $\phi \in \{\pi n/2^{N_w-1} : n = 1, \ldots, 2^{N_w}\}$ and MS uses N_w feedback bits per antenna group for reporting. For amplitude weights v_m, we obtain

$$|\mathbf{g} \cdot \widehat{\mathbf{w}}| = \left| g_1 v_1 + g_2 v_2 e^{j\phi_2} + \ldots + g_L v_L e^{j\phi_L} \right|, \tag{2.4}$$

where v_m is either set to $v_m = \sqrt{1/L}$ or tuned to maximize expected SNR if long-term amplitude information is available in the transmitter side. The MS requires a total of $(L-1)N_w$ feedback bits to report the selected phase weights information for the transmitter.

As we will see later on, compared to the optimal joint phase adjustment, QCP results in insignificant performance degradation while computation complexity and feedback capacity need are smaller. Furthermore, QCP has good implementation flexibility, for instance when using separate control channels towards each antenna groups with different feedback update frequency.

Assuming co-located transmit antennas with homogeneous signal statistics, QCP has been previously investigated for various special cases in terms of number of antenna branches and feedback bits [30,38–41]. Besides, when $L = 2, M = 1$ and $N_w = 2$, QCP resembles closed-loop transmit diversity that is applied in both HSPA and LTE [42], [43]. The only difference between QCP method and the method in HSPA is that in the latter method the feedback word results from the interpolation between two consecutive one-bit feedback words. Yet, from analytical point of view this difference is irrelevant when feedback latency is ignored. QCP can be considered as a 3GPP joint transmission method as data transmission is made from different antenna groups (points).

2.3.3 Ordered quantized co–phasing

To further boost received SNR at the MS, applying short-term amplitude weights in addition to the phase adjustments is a natural extension for QCP. In ordered QCP, best amplitude weights are selected based on short-term order information of signal powers γ_m in addition phase weights that are choosen according to (2.3). Both order and phase information are signaled to the BSs using $\lceil \log_2(L!) \rceil + (L-1)N_w$ feedback bits.

After precoding the received signal is of the form

$$|\mathbf{g} \cdot \widehat{\mathbf{w}}| = |g_{(1)}v_1 + g_{(2)}v_2 e^{j\phi_2} + \ldots + g_{(L)}v_L e^{j\phi_L}|, \tag{2.5}$$

where ϕ_m refers to the advised phase for the m^{th} BS whereas the amplitude weights v_m are selected based on order statistics between signal powers γ_m to maximize expected received signal. Unlike the case of using uniform quantizer for the phase, achieving a suitable amplitude codebook is not trivial for large number of transmit antennas. However, in case of Rayleigh fading for $L = 2$ and $M = 1$, it has been shown for homogeneous channels that $v_1^2 = (1 + (1 + (\pi\rho/2))^2)^{-1/2})/2$, $\rho = \text{sinc}(\pi/2^{N_w})$ and $v_2^2 = 1 - v_1^2$ where $\text{sinc}(x) = \sin(x)/x$ [44].

When $L = 2, M = 1$, and $N_w = 3$ for homogeneous channels, OQCP is similar to the closed-loop mode 2 transmit-diversity that was applied in WCDMA Release 4 system [45]. In this case, there are 16 possible combinations of phase and power adjustments available for selection by the MS, and 3GPP defines power weights as $v_1^2 = 0.8$ and $v_2^2 = 0.2$. We also note that OQCP has also been analytically studied considering identical channel statistics among antenna branches [30, 40]. Similar to QCP, OQCP can be applied as a joint transmission CoMP method.

2.4 Definition of performance measures

2.4.1 Link-level performance measures

To study the performance of CoMP transmission using the hierarchical structure, we use expected SNR, link capacity, BER, fading figure and outage probability as metrics.

Expected SNR that will also be called as SNR gain simply indicates the benefits of a CoMP transmission and it is defined as expected value of the instantaneous SNR [46]:

$$\mathcal{G} = \mathbb{E}\{z\} = \mathbb{E}\{|\mathbf{g} \cdot \widehat{\mathbf{w}}|^2\}. \tag{2.6}$$

Although SNR gain provides information on benefits of the coherent combining, it is not effective in representing the diversity benefit of the CoMP transmission. The diversity benefit is better illustrated using the fading figure, defined by

$$\mathcal{F} = \frac{\mathcal{G}^2}{\mathbb{E}\{z^2\} - \mathcal{G}^2}, \tag{2.7}$$

including the 2^{nd} moment of SNR. When the diversity benefit of the CoMP transmission increases (i.e. received signal variation decreases), fading figure increases from $\mathcal{F} = 1/2$ (attained for one-sided Gaussian fading channel) towards $\mathcal{F} = \infty$ (attained for a static channel).

The other important performance measure we use to provide further insight on coherent combining gain is the average capacity. With constant transmit power and flat fading channel, average capacity (normalized by bandwidth) is of the form

$$C = \mathbb{E}\{\log_2(1+z)\} = \int_0^\infty \log_2(1+z) f(z) dz, \tag{2.8}$$

where z refers to the instantaneous received SNR and the expectation is taken with respect to z using its distribution $f(z)$ [47]. Besides, to reveal more on diversity benefits of the CoMP schemes, we utilize the commonly used metric average BER that is defined as

$$P_e = \int_0^\infty P_{\text{mod}}(z) f(z) dz, \tag{2.9}$$

where $P_{\text{mod}}(\cdot)$ is error rate of the applied modulation scheme [46]. For instance, $P_{\text{mod}}(z) = 1/2 \cdot \text{erfc}(\sqrt{z})$ for the BPSK modulation.

To analyze diversity gain for a combination of Rician and Rayleigh channels, we also apply outage probability that is expressed as the probability of received SNR falls below a given required SNR Z_r:

$$P_o = P(z < Z_r) = \int_0^{Z_r} f(z) dz. \tag{2.10}$$

2.4.2 Link-to-system level mapping

To study the system level performance, we apply the link-to-system level mapping where simulated SINR is mapped to a spectral efficiency $\mathcal{S}$ using an approximation that is based on Shannon formula. This methodology was introduced first time in [48]. Thus, for a given SINR z, the modified Shannon expression is given as

$$\mathcal{S} = \begin{cases} B_{\text{eff}} \log_2\left(1 + z/z_{\text{eff}}\right) & z_{\min} \leqslant z \leqslant z_{\max}, \\ \mathcal{S}_{\max}, & z > z_{\max}, \\ 0, & z < z_{\min}, \end{cases} \tag{2.11}$$

where B_{eff} and z_{eff} account for LTE bandwidth and SINR efficiency, respectively, $z_{\min}$ is the minimum required SINR, $z_{\max}$ is the SINR value providing the maximum spectral efficiency $\mathcal{S}_{\max}$. Once B_{eff} is set based on

amount of overhead used for an LTE configuration, $z_{\min}$ and $z_{\max}$ can be obtained from link-level simulations while z_{eff} is obtained through curve fitting between (2.11) and simulation result [49].

If N_{PRB} is the number of physical resource blocks (PRBs) allocated by a LTE scheduler, then the throughput $\mathcal{T}$ is computed as

$$\mathcal{T} = N_{\text{PRB}} \cdot B_{\text{PRB}} \cdot \mathcal{S}, \tag{2.12}$$

where B_{PRB} is the bandwidth per PRB. In case of half-duplex LTE-A relay, we further modify equation (2.12) to adjust it for the half-duplex nature, as will be explained in Section 5.4.2.

In later sections Monte-Carlo simulation campaigns have been performed to compute the SINR, spectral efficiency and eventually throughputs of UEs (and LPNs) in various scenarios of conventional or heterogeneous network deployments. These system simulation campaigns enable system performance of CoMP methods to be compared amongst each other, as well as, against the benchmark case where CoMP is not used.

3. Hierarchically combined beamforming for CoMP

The hierarchical structure introduced in Section 2.2 enables flexible and effective combination of precoding methods for CoMP system. In [PI], we have made analysis for different combination of TSC and QCP methods. Achieved results are summarized in this chapter.

3.1 System model and assumptions

For the sake of simplicity we have reduced the general system model of Figure 2.1 to $L = 2$ groups of $M = 2$ antennas, as illustrated in Figure 3.1. The antenna pairs can be applied either on different cells of the same site

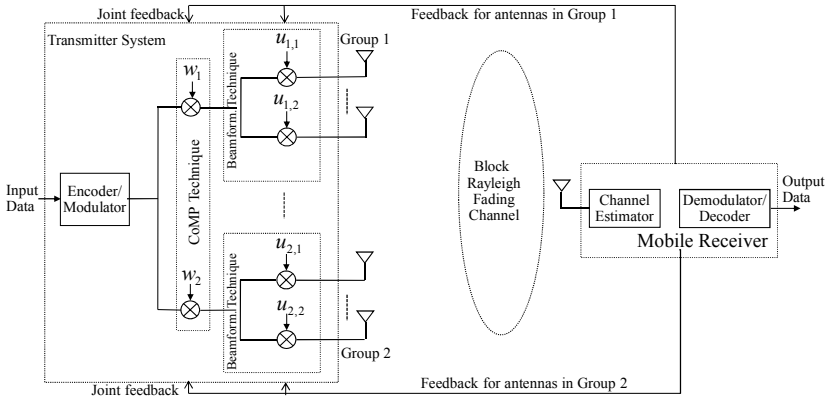

Figure 3.1. Simplified system model of CoMP transmission.

or on separate BS sites. Therefore, the received signal in (2.1) is reduced to the form

$$r[i] = \sum_{m=1}^{2} [(\mathbf{h}_m \cdot \mathbf{u}_m) w_m] s[i] + n[i]. \tag{3.1}$$

In the analysis, the independent channel coefficients $h_{m,k} = \sqrt{\gamma_{m,k}}\, e^{j\psi_{m,k}}$ $(m, k = 1, 2)$ are assumed to be identically distributed such that $\mathbb{E}\{\gamma_{m,k}\} =$

1. The channel coefficients are perfectly known at the receiver side and transmit weights $\mathbf{u}_m$ and $\mathbf{w}$ are selected based on short-term channel state feedback that is available at the transmitter without error or latency. Selected weight vectors $\hat{\mathbf{u}}_m$ and $\hat{\mathbf{w}}$ are known for TSC and QCP algorithms.

3.2 Method combinations

When applying TSC and QCP algorithms within and between the antenna pairs, we end up to four method combinations:

Selection-Selection (SS): Selection scheme is applied both within antenna pairs and between antenna pairs to dynamically determine $\hat{\mathbf{u}}_m$ and $\hat{\mathbf{w}}$, respectively. This approach leads to the use of the antenna with the best channel power which is the same as the traditional TSC. Thus, (2.2) attains the form

$$z_{\mathrm{ss}} = \max\{\gamma_{1,1}, \gamma_{1,2}, \gamma_{2,1}, \gamma_{2,2}\}. \tag{3.2}$$

We need here a total of two feedback bits: one to select an antenna pair and the other to select an antenna from the selected antenna pair. In the following this method is used for benchmarking purposes.

Selection-Quantized Co-phasing (SC): In this approach, QCP is applied in each pair and selection is carried out between pairs. Thus, we select an antenna pair that provides better SNR after QCP. Instantaneous SNR becomes

$$\begin{aligned} z_{\mathrm{sc}} = \max\{&1/2\left(\gamma_{1,1}+\gamma_{1,2}+2\sqrt{\gamma_{1,1}\gamma_{1,2}}\cos\theta_1\right), \\ &1/2\left(\gamma_{2,1}+\gamma_{2,2}+2\sqrt{\gamma_{2,1}\gamma_{2,2}}\cos\theta_2\right)\}, \end{aligned} \tag{3.3}$$

where $\theta_m = \psi_{m,2} - \psi_{m,1} + \phi_m$. The phase $\phi_m = 2(n_m - 1)\pi/2^{N_m}$ refers to the selected phase for the QCP method (see (2.3)) applied in the m^{th} antenna pair with N_m feedback bits. Note that the variable θ_m follows uniform distribution on the range $(-\pi/2^{N_m}, \pi/2^{N_m})$ and SNR values $\gamma_{m,l}$ are independent exponentially distributed variables. This method combination needs a total of $N_m + 1$ feedback bits to be operational. N_m bits for QCP applied in the selected antenna pair and 1 bit for the pair selection.

Quantized Co-phasing-Selection (CS): In this combination, selection is used to determine $\hat{\mathbf{u}}_1$ and $\hat{\mathbf{u}}_2$, and QCP is applied between selected anten-

nas. Hence, instantaneous SNR attains the form

$$z_{\text{cs}} = \frac{1}{2}\left(\gamma_1 + \gamma_2 + 2\sqrt{\gamma_1\gamma_2}\cos\theta_3\right), \tag{3.4}$$

where $\gamma_1 = \max\{\gamma_{1,1}, \gamma_{1,2}\}$, $\gamma_2 = \max\{\gamma_{2,1}, \gamma_{2,2}\}$, and $\theta_w = \psi_2 - \psi_1 + \phi_w \sim U(-\pi/2^{N_w}, \pi/2^{N_w})$. Note that ψ_i denotes the phase of the channel with maximum power and $\phi_w = 2(n_w - 1)\pi/2^{N_w}$ denotes the selected phase for QCP when using N_w phase bits, according to (2.3). Mobile receiver needs to send a total of $N_w + 2$ feedback bits to make CS operational: N_w bits for the QCP and 2 bits for the selections.

Quantized Co-phasing - Quantized Co-phasing (CC): In this case, we define $\hat{\mathbf{u}}_1$, $\hat{\mathbf{u}}_2$ and $\hat{\mathbf{w}}$ based on QCP algorithm. Therefore,

$$z_{\text{cc}} = \frac{1}{4}\left(|z_1|^2 + |z_2|^2 + 2|z_1||z_2|\cos\theta_3\right), \tag{3.5}$$

where $z_m = \sqrt{\gamma_{m,1}} + \sqrt{\gamma_{m,2}}e^{j\theta_m}$. We note that z_m is the resultant signal after QCP is applied at the m^{th} antenna pair using N_m feedback bits. The mutual phase between pairs of signals is given by $\theta_w = \angle z_2 - \angle z_1 + \phi_w$, where θ_w is uniformly distributed on the range $(-\pi/2^{N_w}, \pi/2^{N_w})$ and N_w refers to the number of phase bits when QCP is applied between antenna pairs. This method requires a total of $N_1 + N_2 + N_w$ feedback bits, where N_1 and N_2 denote the number of bits used for the QCPs applied in the first and second antenna pairs and N_w refers to the number of bits used for the QCP between the pairs.

The QCPs that are applied independently in the pairs and between the pairs for CC may use different numbers of feedback bits. On the other hand, CC resembles equal gain transmission when large phase feedback information is available at the transmitter (i.e. $N_1 \gg 1$, $N_2 \gg 1$, and $N_w \gg 1$). We denote this case as CC with large number of feedback bits (CCL).

As noted in the analysis, we treat SS as a reference method since it is equal with the well-studied transmit selection technique from analysis perspective. For comparison purposes, we also recall results when full CSI (FI) is available at transmitter side. It gives performance upper bound while SS gives performance a lower bound.

3.3 Analytical results for SNR gain, fading figure, and BER

This section presents analytical results for SNR gain, fading figure, and BER for the method combinations. We note that more details can be found

from [PI].

3.3.1 SNR gain and fading figure

We recall that SNR gain $\mathcal{G}$ is the first moment and fading figure $\mathcal{F}$ is a function of the first and second moments (see (2.7)). Therefore, to obtain $\mathcal{G}$ and $\mathcal{F}$, we provide derived expressions of the two moments for the method combinations of the Section 3.2.

SS Method: The n^{th} moment for z_{ss} is well-known [47]:

$$\mathbb{E}\{z_{\text{ss}}^n\} = \sum_{i=1}^{2M} \binom{2M}{i} \frac{(-1)^{i+1} n!}{i^n}. \tag{3.6}$$

Here $M = 2$ for the simplified system model.

Full CSI: The instantaneous SNR, denoted by z_{fi}, follows chi-square distribution with $4M$ degrees of freedom and its n^{th} moment has been presented in [47] as

$$\mathbb{E}[z_{\text{fi}}^n] = \frac{\Gamma(2M+n)}{\Gamma(2M)}, \tag{3.7}$$

where $\Gamma(\cdot)$ is the Gamma function. If $M = 2$, then we get $\mathcal{G}_{\text{fi}} = \mathcal{F}_{\text{fi}} = 4$.

SC method: Assuming $x = \gamma_{1,1} + \gamma_{1,2} + 2\sqrt{\gamma_{1,1}\gamma_{1,2}}\cos\theta_1$ and $y = \gamma_{2,1} + \gamma_{2,2} + 2\sqrt{\gamma_{2,1}\gamma_{2,2}}\cos\theta_2$, we have derived moments of z_{sc} by using a distribution formulated from approximate distributions for x and y using error corrected chi-square distribution with 4 degrees of freedom (see Appendix 1 of [PI]). The obtained moments are expressed as

$$\begin{aligned}\mathbb{E}\{z_{\text{sc}}^n\} = &\sum_{i=1}^{3}\sum_{j=1}^{3} \frac{A_{ij}^{xy}(i+n)!}{(2m_x)^{i+n+1}} - B_{ij}^{xy} \sum_{k=0}^{j} \frac{2^{-n}(i+k+n)! m_y^{k-j-1}}{2k!(m_x+m_y)^{i+k+n+1}} \\ &+ \sum_{i=1}^{3}\sum_{j=1}^{3} \frac{A_{ij}^{yx}(i+n)!}{(2m_y)^{i+n+1}} - B_{ij}^{yx} \sum_{k=0}^{j} \frac{2^{-n}(i+k+n)! m_x^{k-j-1}}{2k!(m_x+m_y)^{i+k+n+1}},\end{aligned} \tag{3.8}$$

where $m_p = 2/\mathbb{E}\{p\},\ a_3^p = 4\mathbb{E}\{p^2\}/3\mathbb{E}\{p\}^4 - 2/\mathbb{E}\{p\}^2,\ a_2^p = -3\mathbb{E}\{p\}a_3^p$, and $a_1^p = -\mathbb{E}\{p\}a_2/2 + 1$,

$$A_{ij}^{xy} = \frac{2^{i+1} m_x^2 a_i^x a_j^y j!}{m_y^{j-1}}, \quad B_{ij}^{xy} = 2m_x^2 m_y^2 a_i^x a_j^y j!. \tag{3.9}$$

The first and second moments of x and y have been formulated as

$$\begin{aligned}&\mathbb{E}\{x\} = 2 + \frac{\pi \ \ \text{sinc}(\pi/2^{N_1})}{2}, \quad \mathbb{E}\{y\} = 2 + \frac{\pi\ \text{sinc}(\pi/2^{N_2})}{2}, \\ &\mathbb{E}\{x^2\} = 8 + 2\ \text{sinc}(\pi/2^{N_1-1}) + 3\pi\ \text{sinc}(\pi/2^{N_1}), \\ &\mathbb{E}\{y^2\} = 8 + 2\ \text{sinc}(\pi/2^{N_2-1}) + 3\pi\ \text{sinc}(\pi/2^{N_2}).\end{aligned} \tag{3.10}$$

If $N_1 = N_2$, then $m_x = m_y$, $A_{ij}^{xy} = A_{ij}^{yx}$, $B_{ij}^{xy} = B_{ij}^{yx}$ and (3.8) is reduced to a simple form

$$\mathbf{E}[z_{\rm sc}^n] = 2\sum_{i=1}^{3}\sum_{j=1}^{3}\left(\frac{A_{ij}^{xy}(i+n)!}{(2m_x)^{i+n+1}} - B_{ij}^{xy}\sum_{k=0}^{j}\frac{(i+k+n)!m_x^{k-j-1}}{2^{n+1}k!(2m_x)^{i+k+n+1}}\right). \quad (3.11)$$

CS method: The derived expressions for the first and second moments of $z_{\rm cs}$ have been given as

$$\mathcal{G}_{cs} = \frac{3}{2} + \frac{(2\sqrt{2}-1)^2}{8}\pi\ \mathrm{sinc}(\pi/2^{N_w}), \quad (3.12)$$

$$\mathbb{E}\{z_{\rm cs}^2\} = \frac{7}{4} + \frac{9}{8}(2 + \mathrm{sinc}(\pi/2^{N_w-1})) + \frac{3(17-6\sqrt{2})}{16}\pi\ \mathrm{sinc}(\pi/2^{N_w}). \quad (3.13)$$

CC method: In this case, we have written in [PI] the first and second moments as

$$\mathcal{G}_{\rm cc} = \frac{1}{4}\left[\mathbb{E}\{|z_1|^2\} + \mathbb{E}\{|z_2|^2\} + 2\mathbb{E}\{|z_1|\}\mathbb{E}\{|z_2|\}\mathrm{sinc}(\pi/2^{N_w})\right], \quad (3.14)$$

$$\mathbb{E}\{z_{\rm cc}^2\} = \frac{1}{16}\Big[\mathbb{E}\{|z_1|^4\} + \mathbb{E}\{|z_2|^4\} + 4\mathbb{E}\{|z_1|^3\}\mathbb{E}\{|z_2|\}\mathrm{sinc}(\pi/2^{N_w}) +$$
$$4\mathbb{E}\{|z_1|\}\mathbb{E}\{|z_2|^3\}\mathrm{sinc}(\pi/2^{N_w}) + 2\mathbb{E}\{|z_1|^2\}\mathbb{E}\{|z_2|^2\}\left(2 + \mathrm{sinc}(\pi/2^{N_w-1})\right)\Big]. \quad (3.15)$$

For the even moments we have obtained forms

$$\mathbb{E}\{|z_i|^2\} = 2 + \frac{\pi\ \mathrm{sinc}(\pi/2^{N_i})}{2}, \quad (3.16)$$
$$\mathbb{E}\{|z_i|^4\} = 8 + 3\pi\ \mathrm{sinc}(\pi/2^{N_i}) + 2\mathrm{sinc}(\pi/2^{N_i-1}),$$

and for the odd moments the formula

$$\mathbb{E}\{|z_i|^m\} = \frac{2^{N_i}\Gamma(\frac{m}{2}+2)}{\pi}\sum_{k=0}^{\infty}\frac{(-2)^k\Gamma(\frac{-m}{2}+k)}{k!\,\Gamma(-m/2)}B(\frac{k}{2}+1,\frac{k}{2}+1)I_{N_i}(k), \quad (3.17)$$

was deduced in [PI]. We note that $B(.,.)$ is the beta function as defined in [50, (6.2.1)] and

$$I_{N_i}(k) = \begin{cases} \frac{\pi}{2^{2n+N_i}}\binom{2n}{n} + \frac{1}{2^{2n-1}}\sum_{l=0}^{n-1}\binom{2n}{l}\frac{\sin(2n-2l)\frac{\pi}{2^{N_i}}}{2n-2l}, k = 2n, \\ \\ \frac{1}{2^{2n}}\sum_{l=0}^{n}\binom{2n+1}{l}\frac{\sin(2n-2l+1)\frac{\pi}{2^{N_i}}}{2n-2l+1}, k = 2n+1. \end{cases} \quad (3.18)$$

For large values of N_1, N_2, and N_w CC method is equivalent to the equal gain transmission method, and we have ascertained that

$$\mathcal{G}_{\rm ccl} = \frac{4+3\pi}{4}, \quad \mathbb{E}\{z_{\rm ccl}^2\} = \frac{3\pi^2+108\pi+88}{32}. \quad (3.19)$$

3.3.2 Average bit error rate

We recall that average BER expressions for the reference methods are given by [47]

$$P_e = \begin{cases} \frac{1}{2}\sum_{i=0}^{2M}(-1)^i\binom{2M}{i}\sqrt{\frac{\bar{\gamma}}{\bar{\gamma}+i}}, & \text{for SS,} \\ \left(\frac{1-\sqrt{\bar{\gamma}/(1+\bar{\gamma})}}{2}\right)^{2M}\sum_{i=0}^{2M-1}\binom{2M-1+i}{i}\left(\frac{1+\sqrt{\bar{\gamma}/(1+\bar{\gamma})}}{2}\right)^{i}, & \text{for full CSI,} \end{cases} \tag{3.20}$$

where $\bar{\gamma} = P_t/P_n$ is the average transmit SNR.

For SC method, we have obtained in [PI] a BER expression of the form

$$P_e^{\mathrm{sc}} = \sum_{i=1}^{3}\sum_{j=1}^{3}\left(A_{ij}^{xy}J_{i+1}(2m_x,2\bar{\gamma}) - B_{ij}^{xy}\sum_{k=0}^{j}\frac{2^{i+k}J_{i+k+1}\left(2(m_x+m_y),2\bar{\gamma}\right)}{k!m_y^{j-k+1}}\right) + \sum_{i=1}^{3}\sum_{j=1}^{3}\left(A_{ij}^{yx}J_{i+1}(2m_y,2\bar{\gamma}) - B_{ij}^{yx}\sum_{k=0}^{j}\frac{2^{i+k}J_{i+k+1}\left(2(m_x+m_y),2\bar{\gamma}\right)}{k!m_x^{j-k+1}}\right), \tag{3.21}$$

where A_{ij}^{xy} and B_{ij}^{xy} are given in (3.9) and

$$J_s(a,b) = \frac{\Gamma(s)}{2a^s}\left[1-\sqrt{\frac{b}{b+2a}}\sum_{k=0}^{s-1}\binom{2k}{k}\left(\frac{a}{4a+2b}\right)^k\right]. \tag{3.22}$$

When N_1 is equal to N_2, (3.21) is simplified to

$$P_e^{\mathrm{sc}} = 2\sum_{i=1}^{3}\sum_{j=1}^{3}\left(A_{ij}^{xy}J_{i+1}(2m_x,2\bar{\gamma}) - B_{ij}^{xy}\sum_{k=0}^{j}\frac{2^{i+k}J_{i+k+1}(4m_x,2\bar{\gamma})}{k!m_y^{j-k+1}}\right). \tag{3.23}$$

For both CS and CC method combinations, approximating their SNRs distribution with error corrected chi-square distribution (see Appendix 1 in [PI]), we have achieved a single BER expressions of the form

$$P_e^{\mathrm{mn}} = \frac{128}{3\mathcal{G}_{\mathrm{mn}}^4}\left[a_3J_6\left(\frac{4}{\mathcal{G}_{\mathrm{mn}}},2\bar{\gamma}\right) + a_2J_5\left(\frac{4}{\mathcal{G}_{\mathrm{mn}}},2\bar{\gamma}\right) + a_1J_4\left(\frac{4}{\mathcal{G}_{\mathrm{mn}}},2\bar{\gamma}\right)\right], \tag{3.24}$$

where $\mathrm{mn} \in \{\mathrm{cs},\mathrm{cc}\}$, $J_s(\cdot,\cdot)$ is given in (3.22) and

$$a_3^{\mathrm{mn}} = \frac{32}{5}\frac{\mathbf{E}\left[z_{\mathrm{mn}}^2\right]}{\mathcal{G}_{\mathrm{mn}}^4} - \frac{8}{\mathcal{G}_{\mathrm{mn}}^2}, \quad a_2^{\mathrm{mn}} = -\frac{5}{2}\mathcal{G}_{\mathrm{mn}}a_3^{\mathrm{cs}}, \quad a_1^{\mathrm{mn}} = -\frac{\mathcal{G}_{\mathrm{mn}}}{2}a_2 + 1. \tag{3.25}$$

For CCL, we also use same expressions.

3.4 Performance experiments and observations

3.4.1 SNR gain and fading figure

The SNR gain and the fading figure as a function of number of feedback bits are depicted in Figure 3.2 and Figure 3.3, respectively. Solid curves

represent the analytical results whereas markers refer to the numerical results. For comparison, we also present simulation results for the quantized optimal joint co-phasing (OJC) method where instantaneous SNR is given by

$$z_{\text{ojc}} = \frac{1}{4}\max\{|h_{1,1} + h_{1,2}e^{j\phi_1} + h_{2,1}e^{j\phi_2} + h_{2,2}e^{j\phi_3}|^2, \phi_i = 2(n_i - 1)\pi/2^{N_i}, \\ i \in \{1,2,3\}, n_i \in \{1,2,\ldots,2^{N_i}\}\}.$$

This method selects the best phasing through exhaustive search over all combinations. The result is depicted by dashed curve in the figures. All results are presented assuming $N_1 = N_2 = N_w = N$ and Table 3.1 shows required numbers of feedback bits for SC, CS, and CC as a function of N. We note that SS requires fixed two feedback bits and OJC uses same number of bits with CC. Both Figure 3.2 and Figure 3.3 validates the analytical results presented in Section 3.3.1 showing analytical and simulation results. We note that the performance gap between the lower bound SS and upper bound full CSI case is 2.83dB for the SNR gain and 1.18dB for the fading figure.

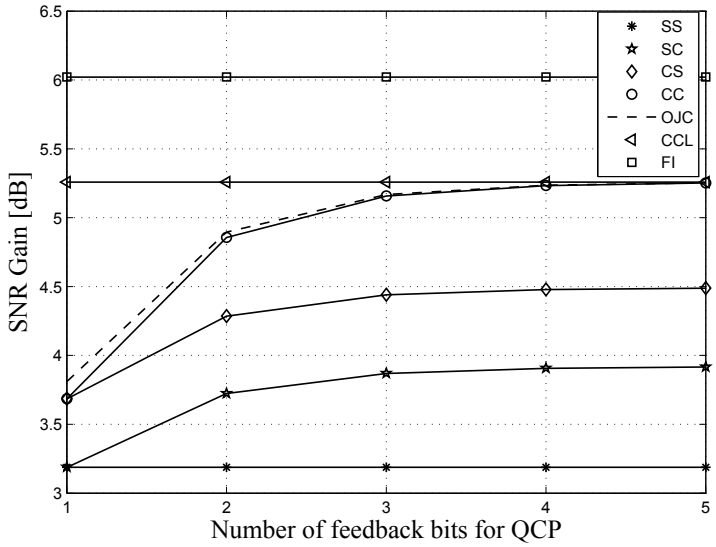

Figure 3.2. SNR gain as a function of the number of feedback bits used for QCP in SC, CS, and CC. Solid curves represent the analytical results where as markers refer to the numerical results; dashed curve refers to the simulation result for OJC. Note that for SS the number of feedback bits is always two and OJC uses same number of bits with CC.

We observe from Figure 3.2 that SNR gain performance for SC, CS, and CC methods converges to 3.9 dB, 4.49 dB, and 5.25 dB, respectively, with

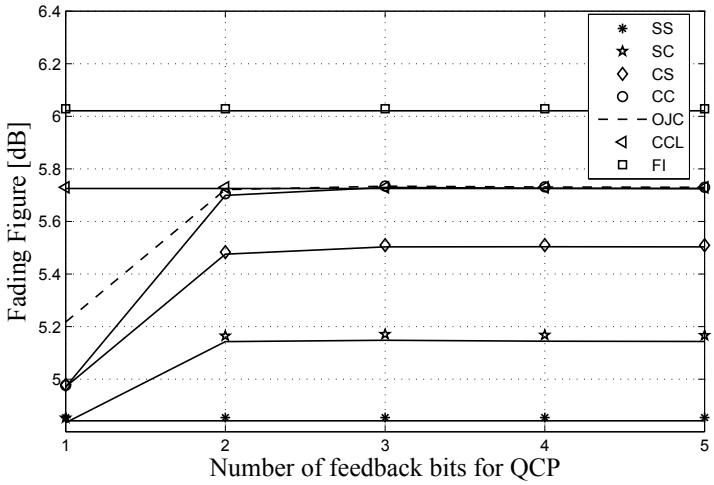

Figure 3.3. Fading figure as a function of the number of feedback bits used for QCP in SC, CS, and CC. Solid curves represent the analytical results where as markers refer to the numerical results; dashed curve refers to the simulation result for OJC. Note that for SS the number of feedback bits is always two and OJC uses same number of bits with CC.

Table 3.1. Total numbers of required feedback bits.

	$N = 1$	$N = 2$	$N = 3$	$N = 4$
SC	2	3	4	5
CS	3	4	5	6
CC	3	6	9	12

only $N = 4$. Increasing N further brings negligible improvement for all methods. We further note that the SNR gain for CC converges to $\mathcal{G}_{\text{ccl}} = (4 + 3\pi)/4$ and the largest improvement for all methods occurs when N increases from 1 to 2. Furthermore, SC and CC perform at the same level as SS and CS, respectively, when $N = 1$; otherwise, the methods perform in the following order: SS, SC, CS, and CC. For instance, when $N = 2$, CC, CS, and SC provide 46.85%, 28.74%, and 13.15% improvement relative to SS while they require 4, 2, and 1 more feedback bits (see Table 3.1), respectively. Moreover, CC shows negligible loss compared to the OJC for $N \geqslant 2$ while both methods require the same number of feedback bits.

For fading figure (see Figure 3.3), we note similar performance trends as those observed in case of SNR gain. We also note that, for instance, when $N = 2$, CC, CS, and SC outperform SS by 0.86 dB, 0.63 dB, and 0.31 dB, respectively.

3.4.2 Average BER

Average BER results are presented in Figure 3.4 and Figure 3.5 when $N = 2$ and $N = 3$, respectively. In both figures analytical results fit well with respective numerical results. Furthermore, we see that the performance order for different methods is the same as in case of SNR gain i.e., FI, CCL, CC, CS, SC and SS. In terms of numerical results we have with $N = 2$, a 2.5 dB, 2.1 dB, 1.4 dB, and 0.7 dB SNR difference for CCL, CC, CS, and SC relative to SS at 10^{-3} average BER value, respectively. We recall here that the CC, CS and SC require 4, 2 and 1 more feedback bits than SS as shown in Table 3.1. Furthermore, we observe that CC curve in both figures overlap with OJC showing negligible performance difference. With $N \geqslant 3$, results of both methods converges to result of CCL which is equivalent to the perfect co-phasing method.

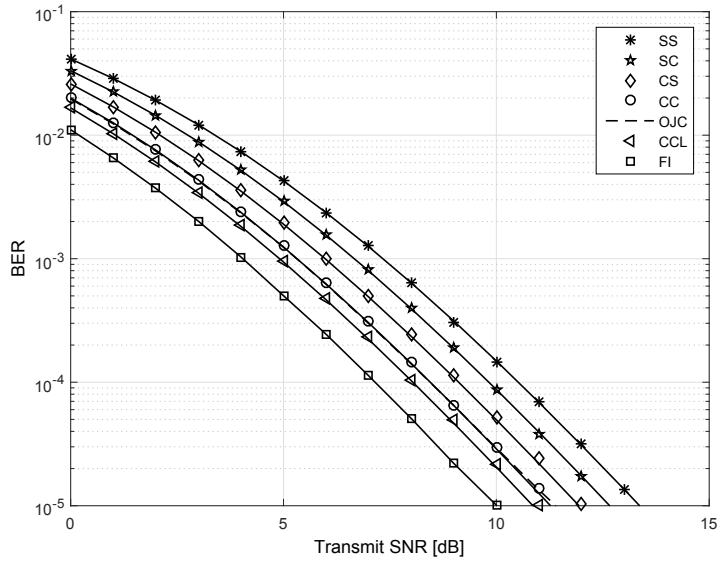

Figure 3.4. Bit error probability as a function of average transmit SNR when $N = 2$. Solid curves refer to the analytical results where as markers refer to the numerical results; dashed curve refers to the simulation result for OJC.

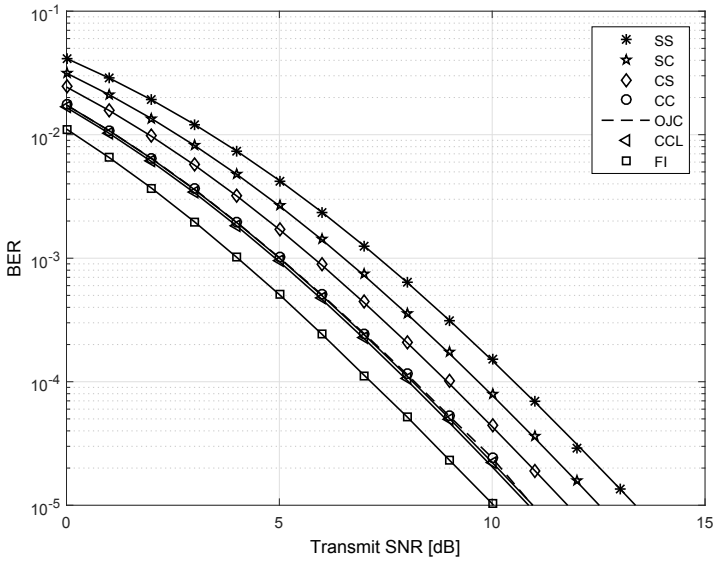

Figure 3.5. Bit error probability as a function of average transmit SNR when $N = 3$. Solid curves refer to the analytical results where as markers refer to the numerical results; dashed curve refers to the simulation result for OJC.

4. Channel power imbalance induced performance loss in CoMP systems

In CoMP transmission systems, a terminal receives multiple copies of the desired signal, with different average power at reception. This is mainly due to channel power imbalance that is mainly resulting from spatially distributed transmissions or different antenna main lobe azimuth directions of different transmitters of the desired signal.

Power imbalance leads to system performance degradation unless receiver design takes the imbalance into account and mitigates its impact. Antenna calibration can be used to address resulting performance deteriorations provided that transmitters are co-located [51]. Yet, it is practically challenging to fully eliminate the power imbalance from among co-located antenna branches due to costs of accurate calibration methods. To that end, the effectiveness of calibration measures is limited and the distributed nature of CoMP makes precise calibration even more complex and impractical. Therefore, power imbalance among transmission points commonly characterizes CoMP systems.

Most of analytical studies on CoMP/MIMO including the investigation in Chapter 3 either assume equalized received powers from different transmission points or completely ignore analysis of performance impact of power imbalance [23]. This shortcoming in literature has motivated our research to thoroughly investigate performance loss incurred in practical limited feedback CoMP methods due to channel power imbalance. Results are presented in detail in [PII,PIII]. While [PII] provides insight into impact of channel power imbalance on benefits of coherent combining, [PIII] presents its impact from the perspective of achieved diversity gain. In both cases the findings are presented based on derived mathematical expressions for SNR gain, amplitude weights, average capacity, and average BER. Detailed derivations and interpretations are reported in the publications.

In this chapter, we partly recall and extend the discussion on channel power imbalance scenarios presented in publication [PII], and provide an overview of system model and studied CoMP techniques. Then concise summary of achieved results on impacts of channel power imbalance for the different CoMP techniques and reference schemes are presented. Concluding discussion on power imbalance impacts is carried out at the end of the chapter.

4.1 Practical scenarios with channel power imbalance

The need to study effects channel power imbalance is not only motivated in CoMP deployment scenarios in LTE-A and future mobile systems, but also for the case of DAS and co-located multi-antenna systems.

4.1.1 The 3GPP CoMP scenarios

As it has been explained in [13, 14], 3GPP has evaluated selected CoMP deployment scenarios under both homogeneous and heterogeneous networks assuming ideal and imperfect backhaul among transmission points in a CoMP set. In CoMP JP, data to a CoMP user is sent from all CoMP transmission points. In 3GPP CoMP scenario 1 or 2, the CoMP operation takes place among co-located or distributed macro BSs, respectively [13] or in small cell enhancement scenario 2a the coordination may be executed among LPNs [14]. The CoMP operation can also be carried out between a macrocell and LPNs in case of small cell enhancement scenario 1 [14].

With the exception of CoMP scenario 1, the macrocells or/and LPNs within CoMP set are usually assumed to be at different locations. Therefore, the CoMP user experiences different distance dependant and shadowing pathloss from the transmission points. This pathloss difference resulting from distributed transmissions leads to power imbalance at reception. In CoMP scenario 1 we have adjacent sectors with different logical cells controlled by the same network element. This scenario is convenient for CoMP techniques under JP categories as it has no backhaul limitations for coordination. Even in this scenario, power imbalance occurs among the received signals mainly because antenna main lobes of the sectors are directed differently.

4.1.2 Distributed antenna systems

Unlike conventional MIMO system, DAS architecture consists of geographically distributed antennas connected to centrally controlling network element. The DAS systems were originally introduced in late 1980s to improve indoor coverage [52] and they were later widely deployed to boost system capacity in hotspot areas. Considerable advantages can be obtained from the distributed antenna architecture by applying suitable transmission techniques. The performance improvements for various methods have been investigated and results presented in literature [20, 53–55]. Due to the spatially distributed transmissions inherent to DAS system, problem of power imbalance among received signals from the multiple antennas is experienced.

4.1.3 Co-located multi-antenna systems with errors

In traditional MIMO systems, multiple co-located antennas are used to enhance system capacity by exploiting diversity or multiplexing data streams [56, 57]. Various MIMO features have been introduced into contemporary mobile standards. For instance, LTE-A supports upto 8x8 MIMO although manufacturing a mobile terminal with eight antennas is practically challenging due to size limitations and affordability [58]. In research it is common to assume accurate implementation of transmission-reception chain of such multi-antenna systems so that signals from transmit antennas admit similar statistical properties at reception. In practice, imperfect implementation of the antenna chains might be the case especially in base stations. There could be implementation errors in calibration of power amplifier, antenna cabling, and antenna pattern orientation. As a result, notable received power imbalance among transmissions from co-located antennas may exist. The amount depending on the level of imperfection of the transmitter chain implementation.

4.2 System model and assumptions

The channel power imbalance impacts have been studied using the system model depicted in Figure 4.1, which is derived from the generalized CoMP system model presented in Figure 2.1. It is composed by two groups of M antenna branches that transmit the same data to a user with single

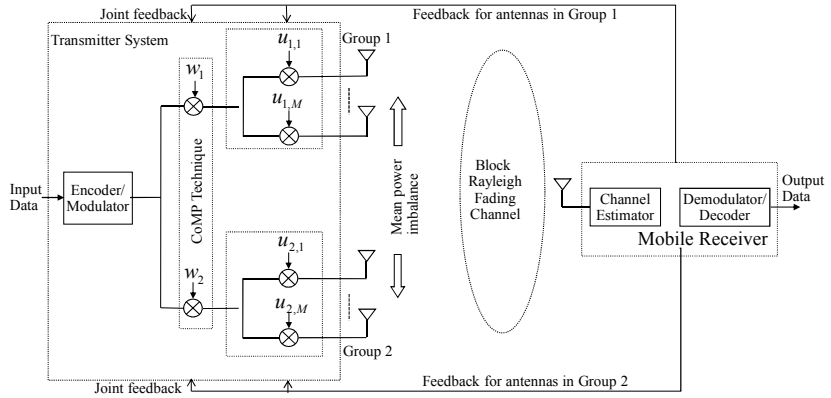

Figure 4.1. System model that is composed by groups of transmit antennas. Antenna groups serve two cells either in geographically distributed sites or same site.

antenna receiver. The antenna groups serve either two geographically separated sites as in inter-site CoMP or adjacent sectors of a multi-sector BS as in intra-site CoMP. Hence, as in (2.1) the received signal at a given time instant can be written as

$$r = \sum_{m=1}^{2} \left[(\mathbf{h}_m \cdot \mathbf{u}_m) w_m \right] s + n, \tag{4.1}$$

where the independent channel coefficients $h_{m,k}$ of the vector $\mathbf{h}_m$ are related to antenna branches from different groups (or BSs) such that $\mathbb{E}\{\gamma_{m,k}\} = \bar{\gamma}_m$ and $\bar{\gamma}_m \neq \bar{\gamma}_{m'}$ if $m \neq m'$. Yet, negligible imbalance is considered among antenna branches of the same BS assuming accurate antenna calibration. The MS admit accurate CSI and it provides both short-term and long-term feedback to transmission points using error-free and delay-free feedback channels. Furthermore, we have assumed perfect knowledge of long-term channel strength at the transmitter side.

4.3 CoMP methods

The performance loss analysis has been carried out for TSC, QCP, and OQCP CoMP techniques while an M-antenna QCP scheme with equal long-term amplitude weights is assumed within the groups. Thus, applied weight $\hat{\mathbf{u}}_m$ in (4.1) is chosen based on M-antenna QCP operation within the m^{th} group using $(M-1)N_m$ feedback bits. Furthermore, the weight vector $\hat{\mathbf{w}}$ for the CoMP methods are selected according to the following algorithms:

TSC CoMP: $|\mathbf{g} \cdot \widehat{\mathbf{w}}| = \max\{\sqrt{\gamma_m} : m = 1, 2\}$. Note that here vector g consists of components $g_m = \mathbf{h}_m \cdot \widehat{\mathbf{u}}_m = \sqrt{\gamma_m} e^{j\psi_m}$.

QCP CoMP: $|\mathbf{g} \cdot \widehat{\mathbf{w}}| = \max\left\{\left|g_1 v_1 + g_2 v_2 e^{j\phi_n}\right| : n = 1, \ldots, 2^{N_w}\right\}$, where $\phi_n = \pi n / 2^{N_w - 1}$ for N_w feedback bits and v_1, v_2 refer to long-term transmit weights that maximize expected SNR. We set $v_1 = v_2 = \sqrt{1/2}$ if long-term amplitude information is not exploited.

OQCP CoMP: $|\mathbf{g} \cdot \widehat{\mathbf{w}}| = |g_{(1)} v_1 + g_{(2)} v_2 e^{j\hat{\phi}_n}|$, where $\hat{\phi}_n$ refers to the best phase based on QCP whereas v_1 and v_2 are expected SNR maximizing weights. The amplitude weights are selected based on long-term amplitude information and short-term order statistics between powers γ_1 and γ_2.

We recall that deducing usable exact distribution of γ_m has not been feasible. Therefore, we have applied approximation where chi-square distribution with $2M$ degrees of freedom is scaled by $\mathbb{E}\{\gamma_m\} = \bar{\gamma}_m \mathcal{G}_c$, $\bar{\gamma}_m$ being the common average channel power of each antenna branch in the m^{th} group. Exact expression for $\mathcal{G}_c$ can be recalled from [44]:

$$\mathcal{G}_c = 1 + \frac{M-1}{2M}\left(1 + \frac{M-2}{2}\text{sinc}(\frac{\pi}{2^{N_\text{u}}})\right)\pi\ \text{sinc}(\frac{\pi}{2^{N_\text{u}}}). \tag{4.2}$$

The approximation employs the fact that γ_m follows chi-square distribution when full CSI is applied within the groups. The approximated chi-square distribution demonstrates an average accuracy level more than 98% with respect to distribution of the numerical results of γ_m irrespective of M and becomes exact when $M = 1$.

Without loss of generality we have also assumed that $\bar{\gamma}_1 > \bar{\gamma}_2$ and $v_1 > 0$ in the analysis and denoted that power imbalance between the antenna groups by $\sigma_0 = \bar{\gamma}_2 / \bar{\gamma}_1$. Hereafter, we present the expressions for different performance metrics as a function of σ_0. The intensive mathematical analysis that led us to the results can be recalled from [PII, PIII] where all intermediate steps of the analysis are clearly presented.

4.4 Analytical results for the performance measures

Closed-form expression for the capacity and BER can be derived when the distribution $f(z)$ of SNR is known and (2.8) and (2.9) are analytically integrable. This is the case if the perfect CSI is available or TSC is applied. However, for QCP and OQCP algorithms the distribution $f(z)$ is difficult to obtain but it tuns out that we can compute for both algorithms the *asymptotic* capacity and BER in closed-form.

In the following we first deduce expressions for weights that are optimal with respect to SNR, then the derivations for capacity and BER have been made. Results presented in the following subsections are valid for any normalized weights.

4.4.1 Optimal amplitude weights and SNR gain

Irrespective of the applied CoMP methods, the instantaneous received SNR can be written as

$$z = v_1^2\gamma_{(1)} + v_2^2\gamma_{(2)} + 2v_1v_2\sqrt{\gamma_{(1)}\cdot\gamma_{(2)}}\cos\theta, \tag{4.3}$$

where $\gamma_{(1)} = \max\{\gamma_1, \gamma_2\}$, $\gamma_{(2)} = \min\{\gamma_1, \gamma_2\}$ and θ represents the residual phase difference in reception. Obviously, $v_1 = 1$ and $v_2 = 0$ for TSC whereas $\theta = 0$ and $v_m = \sqrt{\gamma_m/(\gamma_m + \gamma_{3-m})}$ for the full CSI case. The SNR gain $\mathcal{G}$ for these reference methods is obtained by computing expected values of maximum and sum of the two chi-square variables:

$$\mathcal{G} = \begin{cases} \mathcal{G}_c\bar{\gamma}_1(1+\sigma_0), & \text{for full CSI} \\ \mathcal{G}_c\bar{\gamma}_1\left(1+\sigma_0-\kappa_2(\sigma_0)\right) & \text{for TSC,} \end{cases} \tag{4.4}$$

where the expression for $\mathcal{G}_c$ is given by (4.2) and

$$\kappa_2(\sigma_0) = \sum_{k=0}^{M-1}\frac{\Gamma(M+k+1)}{M\Gamma(M)k!}\left(\frac{\sigma_0^{M+1}+\sigma_0^{k+1}}{(1+\sigma_0)^{M+k+1}}\right), \tag{4.5}$$

is the term quantifying the performance loss of TSC relative to the full CSI case.

For QCP, we have achieved in [PII] expressions for the weights maximizing the SNR gain:

$$v_2^2 = \frac{\left(\sigma_0 - 1 + \sqrt{(1-\sigma_0)^2 + 4\kappa_1^2\sigma_0}\right)^2}{\left(\sigma_0 - 1 + \sqrt{(1-\sigma_0)^2 + 4\kappa_1^2\sigma_0}\right)^2 + 4\kappa_1^2\sigma_0}, \quad v_1^2 = 1 - v_2^2, \tag{4.6}$$

where $\kappa_1 = \Gamma(M+1/2)^2/(M\Gamma(M)^2)\text{sinc}(\pi/2^{N_w})$. We note that while phase adjustments are carried out in short-term fashion, the weights (4.6) are based on only long-term average channel powers of the groups. The corresponding SNR gain expression is given by

$$\mathcal{G} = \frac{\mathcal{G}_c\bar{\gamma}_1}{2}\left(1+\sigma_0+\sqrt{(1-\sigma_0)^2+4\kappa_1^2\sigma_0}\right). \tag{4.7}$$

Furthermore, derived expressions of the weights maximizing the SNR

gain for OQCP were in [PII] given as

$$v_2^2 = \frac{4\kappa_1^2\sigma_0}{4\kappa_1^2\sigma_0 + \left(1+\sigma_0-2\kappa_2(\sigma_0)+\sqrt{\left(1+\sigma_0-2\kappa_2(\sigma_0)\right)^2+4\kappa_1^2\sigma_0}\right)^2},$$
$$v_1^2 = 1 - v_2^2, \tag{4.8}$$

and the SNR gain attains the form

$$\mathcal{G} = \frac{\mathcal{G}_c\bar{\gamma}_1}{2}\left(1+\sigma_0+\sqrt{\left(1+\sigma_0-2\kappa_2(\sigma_0)\right)^2+4\kappa_1^2\sigma_0}\right). \tag{4.9}$$

We emphasize that the weights in case of OQCP are selected based on both long-term average channel power and short-term order information such that v_1 is applied to the group with maximum instantaneous sum signal power.

4.4.2 Asymptotic capacity formulae

The average capacity normalized by bandwidth attains the form $C = E\{\log_2(1+z)\}$, where z is the SNR expressed in (4.3). For benchmarking purpose, we formulate first the asymptotic capacity for the case where short-term CSI is not available (i.e. $z = \gamma_1$):

$$\lim_{\bar{\gamma}_1\to\infty}(C - \log_2(\bar{\gamma}_1)) = -\log_2(e)\left(e_c - \log(\frac{\mathcal{G}_c}{M}) - \delta(M)\right), \tag{4.10}$$

where e_c is the Euler constant, $\delta(M) = \sum_{k=1}^{M-1}\frac{1}{k}$ for $M > 1$ and $\delta(1) = 0$. We have recalled (4.10) in order to show the asymptotic difference between the capacity of the precoded channel and the AWGN channel capacity. If $M = 1$, then we have the Rayleigh fading case and (4.10) is reduced to the form

$$\lim_{\bar{\gamma}_1\to\infty}(C - \log_2(\bar{\gamma}_1)) = -\log_2(e)e_c, \tag{4.11}$$

which was previously presented in [59]. In [PII] we have derived expression of the asymptotic capacity for the full CSI case:

$$\lim_{\bar{\gamma}_1\to\infty}(C - \log_2(\bar{\gamma}_1)) = -\frac{\log_2(e)}{\Gamma(M)}\sum_{m=1}^{2}\left[\sum_{k=0}^{M-1}\frac{(2(M-1)-k)!}{(M-1-k)!}\right.$$
$$\left.\frac{(1-\sigma_0^{2m-3})^{k+1-M}}{\left(1-\sigma_0^{3-2m}\right)^M}[e_c + \log(\frac{M}{\mathcal{G}_c\sigma_0^{m-1}}) - \delta(k+1)]\right], \tag{4.12}$$

and for TSC:

$$\lim_{\bar{\gamma}_1\to\infty}(C-\log_2(\bar{\gamma}_1)) = -\log_2(e)\sum_{m=1}^{2}\Bigg[\left(e_c+\log\left(\frac{M}{\mathcal{G}_c\sigma_0^{2-m}}\right)-\delta(M)\right) - \sum_{k=0}^{M-1}\frac{\Gamma(M+k)}{\Gamma(M)k!}\frac{\sigma_0^{M(m-1)+k(2-m)}}{(1+\sigma_0)^{M+k}}\times \left(e_c+\log\left(\frac{M(1+\sigma_0)}{\mathcal{G}_c\sigma_0}\right)-\delta(M+k)\right)\Bigg]. \quad (4.13)$$

If we set $M=1$, then (4.12) and (4.13) become

$$\lim_{\bar{\gamma}_1\to\infty}(C-\log_2(\bar{\gamma}_1)) = \begin{cases} -\log_2(e)\left(e_c+\frac{\sigma_0\log\sigma_0}{1-\sigma_0}\right), & \text{for full CSI,}\\ -\log_2(e)\left(e_c-\log(1+\sigma_0)\right), & \text{for TSC,}\end{cases} \quad (4.14)$$

and by comparing (4.11) and (4.14) we find that the asymptotic capacity going with respect to Rayleigh fading case is of the form

$$\Delta C = \begin{cases} -\log_2(e)\frac{\sigma_0\log\sigma_0}{1-\sigma_0}, & \text{for full CSI,}\\ \log_2(e)\log(1-\sigma_0), & \text{for TSC.}\end{cases} \quad (4.15)$$

For QCP, we have achieved in [PII] an asymptotic capacity of the form

$$\lim_{\bar{\gamma}_1\to\infty}(C-\log_2(\bar{\gamma}_1)) = 2\log_2 v_1 - \frac{\log_2(e)}{\Gamma(M)}\sum_{m=1}^{2}\Bigg[\sum_{k=0}^{M-1}\frac{(2(M-1)-k)!}{(M-1-k)!} \frac{\left(1-(\frac{v_2^2\sigma_0}{v_1^2})^{2m-3}\right)^{k+1-M}}{\left(1-(\frac{v_2^2\sigma_0}{v_1^2})^{3-2m}\right)^{M}}\left(e_c+\log\left(\frac{M}{\mathcal{G}_c(\frac{v_2^2\sigma_0}{v_1^2})^{m-1}}\right) - \delta(k+1)\right)\Bigg] - \log_2(e)\sum_{n=1}^{\infty}\frac{(-1)^n}{n}A_nB_n^{\infty}, \quad (4.16)$$

where

$$A_n = \begin{cases} \binom{n}{n/2}\frac{\pi}{2^{N_w+n}} + \frac{1}{2^{n-1}}\sum_{k=0}^{n/2-1}\binom{n}{k}\frac{\sin\left(\frac{(n-2k)\pi}{2^{N_w}}\right)}{n-2k}, & n=\text{even},\\ \frac{1}{2^{n-1}}\sum_{k=0}^{(n-1)/2}\binom{n}{k}\frac{\sin\left(\frac{(n-2k)\pi}{2^{N_w}}\right)}{n-2k}, & n=\text{odd},\end{cases} \quad (4.17)$$

$$B_n^{\infty} = \frac{2^n\Gamma(2M)}{\Gamma(M)^2}\left(\frac{\sigma_0 v_2^2}{v_1^2}\right)^M B\left(M+\frac{n}{2},M+\frac{n}{2}\right) \times {}_2F_1\left(2M,M+\frac{n}{2};2M+n;1-\frac{v_2^2}{v_1^2}\sigma_0\right). \quad (4.18)$$

The ${}_2F_1$ is the confluent hypergeometric function. We note that for $M=1$, (4.16) attains the form

$$\lim_{\bar{\gamma}_1\to\infty}(C-\log_2(\bar{\gamma}_1)) = -\log_2(e)\left[e_c-2\log v_1+\frac{\sigma_0 v_2^2\log\sigma_0 v_2^2/v_1^2}{v_1^2-v_2^2\sigma_0}+ \sum_{n=1}^{\infty}\frac{(-1)^n}{n}A_nB_n^{\infty}\right] = -\log_2(e)e_c+\Delta C, \quad (4.19)$$

where A_n and B_n^{∞} are evaluated with $M = 1$ and ΔC refers to the asymptotic capacity gain against SISO Rayleigh fading channel.

In case of OQCP, the asymptotic capacity in [PII] had been formulated as

$$\lim_{\bar{\gamma}_1\to\infty}(C - \log_2(\bar{\gamma}_1)) = \log_2(e)\Bigg[\delta(2M) - e_c + \log\left(\frac{\mathcal{G}_c}{M}\right) - \frac{\Gamma(2M)\sigma_0^M}{\Gamma(M)^2}\Bigg(L_0(1,\sigma_0,1,\sigma_0) + L_0(\sigma_0,1,\sigma_0,1) - L_0(\sigma_0 v_2^2, \sigma_0 v_1^2, 1, \sigma_0) - L_0(\sigma_0 v_2^2, \sigma_0 v_1^2, \sigma_0, 1)\Bigg) - \sum_{n=1}^{\infty}\frac{(-1)^n}{n} A_n \cdot {}_oB_n^{\infty}\Bigg], \tag{4.20}$$

where A_n is given by (4.17),

$${}_oB_n^{\infty} = \frac{2\Gamma(2M)(\frac{2v_2}{v_1})^n}{\Gamma(M)^2(n+2M)\sigma_0^M}\Bigg[F_1\left(\frac{n+2M}{2}, n, 2M, M+1+\frac{n}{2}; -\frac{v_2^2}{v_1^2}, -\frac{1}{\sigma_0}\right) + \sigma_0^{2M} F_1\left(\frac{n+2M}{2}, n, 2M, M+1+\frac{n}{2}; -\frac{v_2^2}{v_1^2}, -\sigma_0\right)\Bigg], \tag{4.21}$$

and for a given M we find expression for $L_0(a,b,c,d) = \int_0^1 \frac{t^{M-1}\log(ax+b)}{(cx+d)^{2M}}dx$ using a recursive formula presented in Appendix A of [PII]. The F_1 is the hypergeometric function of two variables. We note that for $M = 1$, (4.20) can be written in the form $\lim_{\bar{\gamma}_1\to\infty}(C - \log_2(\bar{\gamma}_1)) = -\log_2(e)e_c + \Delta C$, where term ΔC defines the OQCP gain in terms of the asymptotic capacity. The explicit expression for ΔC can be obtained using (4.17) and (4.21) by setting $M = 1$, and

$$L_0(a,b,c,d) = \frac{\log(b)}{cd} - \frac{\log(a+b)}{c(c+d)} + \frac{a}{bcd}F_1\left(1,1,1,2; \frac{-a}{b}, \frac{-c}{d}\right). \tag{4.22}$$

4.4.3 Bit error rate formulae

We have derived exact asymptotic and approximate BER expressions for $M = 1$ in [PIII] while BER analysis for general M is left for future work. We note that derivations can be done using the similar methodology applied for capacity in [PII].

Asymptotic BER

The attained asymptotic BER results for $M = 1$ can be generally written in the form

$$\log_{10} P_e(\bar{\gamma}_1, \bar{\gamma}_2) = M(\sigma_0) - 2 \cdot \log_{10}\bar{\gamma}_1, \qquad \bar{\gamma}_1 \gg 1, \tag{4.23}$$

where $M(\sigma_0)$ is not depending on $\bar{\gamma}_1$ but just on the ratio σ_0. Formula (4.23) shows that the diversity gains of the CoMP methods are equal

to two despite the mean power imbalance. For the full CSI case and TSC, expressions for $M(\sigma_0)$ became

$$M(\sigma_0) = \begin{cases} \log_{10}(3/(16\sigma_0)), & \text{for full CSI,} \\ \log_{10}(3/(8\sigma_0)), & \text{for TSC.} \end{cases} \tag{4.24}$$

The asymptotic BER derivation for QCP in [PIII] shows that

$$M(\sigma_0) = \log_{10}\left(3/(16\sigma_0) \cdot A_{N_{\text{rp}}}(v_1, v_2)\right), \tag{4.25}$$

where

$$A_{N_{\text{rp}}}(v_1, v_2) = \frac{1}{2v_1^2 v_2^2}\left[\csc^2\left(\frac{\pi}{2^{N_w}}\right) - \frac{2^{N_w}}{\pi}\cot\left(\frac{\pi}{2^{N_w}}\right)\right]. \tag{4.26}$$

Optimal asymptotic BER is achieved when $v_1 = v_2 = \sqrt{1/2}$ irrespective of value of σ_0 as can be seen from (4.26).

For OQCP, we have obtained in [PIII]

$$M(\sigma_0) = \log_{10}\left(3/(8\sigma_0) \cdot B_{Nw}(v_1, v_2)\right), \tag{4.27}$$

where

$$B_{Nw}(v_1, v_2) = \sum_{n=0}^{\infty} \frac{2^{(N_w+1)}(-2)^n(n+1)v_2^n}{\pi(n+2)v_1^{n+4}}\left[A_n + \frac{1}{2^{n-1}}\sum_{k=0}^{B_n}\binom{n}{k}\frac{\sin\left(\frac{(n-2k)\pi}{2^{N_w}}\right)}{n-2k}\right]$$
$$ {}_2F_1(n+2, \frac{n}{2}+1; \frac{n}{2}+2; \frac{-v_2^2}{v_1^2}). \tag{4.28}$$

In this formula $A_n = \binom{n}{n/2}\pi/2^{N+n}$ and $B_n = n/2 - 1$ for even n and $A_n = 0$ and $B_n = (n-1)/2$ for odd n.

BER for low-to-moderate SNR region

The BER results for the reference no CSI and full CSI cases are well-known from literature and can be formulated as

$$P_e = \begin{cases} \frac{1}{2}\left[1 - \sqrt{\frac{\bar{\gamma}_1}{1+\bar{\gamma}_1}}\right], & \text{for no CSI} \\ \frac{1}{2}\left[1 - \frac{1}{1-\sigma_0}\sqrt{\frac{\bar{\gamma}_1}{1+\bar{\gamma}_1}}\left(1 - \sigma_0\sqrt{\frac{\sigma_0(1+\bar{\gamma}_1)}{1+\sigma_0\bar{\gamma}_1}}\right)\right], & \text{for full CSI.} \end{cases} \tag{4.29}$$

The TSC has also been well studied in literature [60, 61] and its BER can be written in the form

$$P_e = \frac{1}{2}\left[1 - \sqrt{\frac{\bar{\gamma}_1}{1+\bar{\gamma}_1}} - \sqrt{\frac{\bar{\gamma}_1\sigma_0}{1+\bar{\gamma}_1\sigma_0}} + \sqrt{\frac{\bar{\gamma}_1\sigma_0}{1+\sigma_0(1+\bar{\gamma}_1)}}\right]. \tag{4.30}$$

We have derived approximate BER expressions for QCP and OQCP in [PIII] based on their asymptotic BER expressions and SNR gain presented above and in Section 4.4.1. The SNR distributions of both QCP and

OQCP are approximated by sum of two exponential distributions with parameters selected to fit the corresponding expressions of asymptotic BER and SNR gain. Then using the approximated distribution for both methods we are able to formulate P_e as

$$P_e = \frac{1}{2}\left[1 - \frac{1}{1-\sigma_0/C_{N_w}}\sqrt{\frac{\mathcal{L}\bar{\gamma}_1}{1+\sigma_0/C_{N_w}+\mathcal{L}\bar{\gamma}_1}} \left(1 - \frac{\sigma_0}{C_{N_w}}\sqrt{\frac{1+\sigma_0/C_{N_w}+\mathcal{L}\bar{\gamma}_1}{1+C_{N_w}/\sigma_0+\mathcal{L}\bar{\gamma}_1}}\right)\right], \tag{4.31}$$

where $C_{N_w}(v_1, v_2) = A_{N_w}(v_1, v_2)$ for QCP, $C_{N_w}(v_1, v_2) = 2B_{N_w}(v_1, v_2)$ for OQCP and

$$\mathcal{L} = \begin{cases} \frac{1}{2}\left[1+\sigma_0+\sqrt{(1-\sigma_0)^2+\frac{\sigma\pi^2}{4}\text{sinc}(\frac{\pi}{2^{N_w}})}\right], & \text{for QCP}, \\ \frac{1}{2}\left[1+\sigma_0+\sqrt{(\frac{1+\sigma_0^2}{1+\sigma_0})^2+\frac{\sigma\pi^2}{4}\text{sinc}(\frac{\pi}{2^{N_w}})}\right], & \text{for OQCP}. \end{cases}$$

We note that this formula is valid if $\sigma_0 < C_{N_w}$. Yet, this is not a limitation since A_{N_w} and $2B_{N_w}$ are both larger than one. To the best of our knowledge, this approximation has been previously used only in [62] and we can derive average capacity for low-to-moderate SNR region using the same methodology.

4.5 Validations and performance evaluations

4.5.1 Optimal transmit weights

Figure 4.2 presents the power ratio v_1^2/v_2^2 between the optimal transmit weight coefficients (see (4.6) and (4.8)) as a function of σ_0 for $M = 1$ when $N_u = 2$, and number N_w of phase bits is 1, 2, and 3. The ratio increases as expected when σ_0 decreases and order information used in OQCP does not have significant impact on the power ratio when σ_0 is very small. Yet, OQCP is more attractive if σ_0 is varying as it shows smaller power ratio variation compared to QCP. Furthermore, in [PII] we have shown (see Figure 7 therein) that when M increases the power ratio gap between QCP and OQCP becomes negligible since antenna diversity decreases fast variation of received sum signal.

4.5.2 SNR gain

The SNR gain (i.e. $\mathcal{G}$) as a function of σ_0 for $M = 1$ and $\bar{\gamma}_1 = 0$ dB is depicted in Figure 4.3. The markers refer to the numerical results whereas

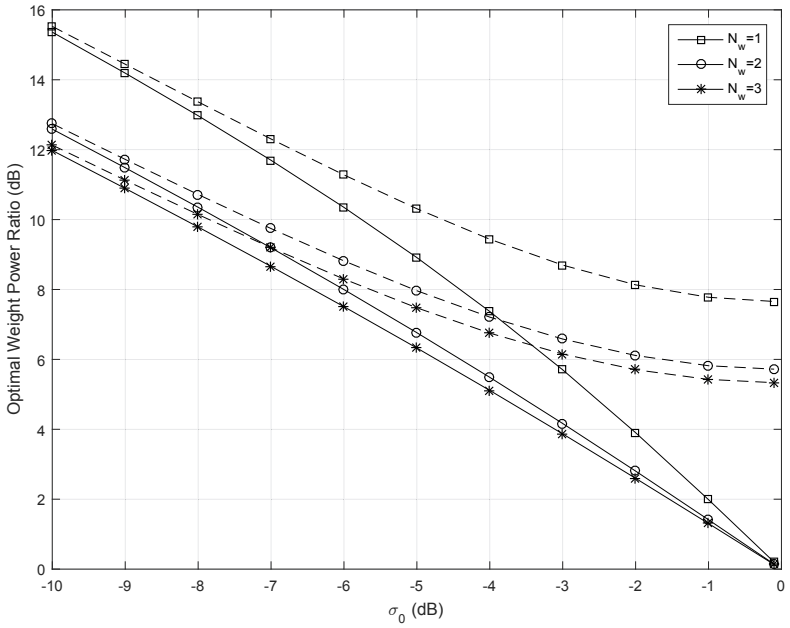

Figure 4.2. Power ratio v_1^2/v_2^2 between the optimal transmit weights as a function of σ_0 for QCP (solid curves) and OQCP (dashed curves) when $M = 1$. Curves with squares, circles and stars refer to $N_w = 1$, 2 and 3 phase feedback bits, respectively.

solid curves refer to the analytical results presented in (4.4), (4.7), and (4.9). The QCP is also plotted without exploiting long-term amplitude feedback when $v_1 = v_2 = \sqrt{1/2}$ and $\mathcal{G} = \mathcal{G}_c\bar{\gamma}_1(1 + \sigma_0 + 2\kappa_1\sqrt{\sigma_0})/2$. The numerical results clearly fit corresponding analytical results validating their derivations.

We see that when σ_0 decreases, the SNR gain loss is experienced in all schemes. For instance, SNR gain reductions of 22.2%, 23.7%, 25.0%, and 25.0% are seen for TSC, QCP, OQCP, and full CSI case, respectively, when power imbalance increases from 0 dB to 3 dB. We note that QCP performs even worse than TSC for large power imbalance when not exploiting long-term amplitude feedback. Furthermore, the larger the imbalance, the smaller the performance difference between QCP and OQCP. We also recall from [PII] (see Figure 9) that when M increases both QCP and OQCP perform very close to full CSI case for wider range of σ_0 and the performance difference between them becomes small.

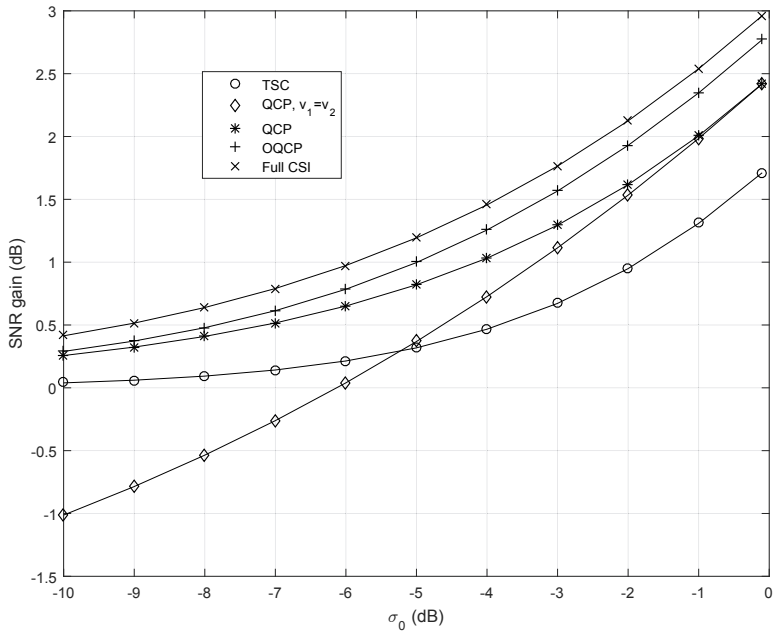

Figure 4.3. SNR gain in terms of the mean power ratio σ_0 when $M = 1$, $N_w = 3$ and $N_{\mathrm{u}} = 2$. Solid curves refer to the analytical results and markers refer to the numerical results.

4.5.3 Average capacity

The capacity loss due to power imbalance is depicted in Figure 4.4 where asymptotic capacity is presented as a function of σ_0 for $M = 1$ assuming $\bar{\gamma}_1 = 30$ dB. Solid curves refer to the analytical results and the markers refer to the numerical results. The visible match between analytical and numerical results is validating the asymptotic capacity expressions presented in (4.12), (4.13), (4.16), and (4.20).

Figure 4.4 also shows that, similar to the case of SNR gain, QCP without long-term amplitude weights performs worse than TSC for large imbalance. For both QCP and OQCP, it is observed that the capacity performance degrades with increasing imbalance. It is also noted that OQCP consistently outperforms QCP. We recall from [PII](Figure 5) that both techniques perform closer to the full CSI case when number of antennas in BSs is increased. On the other hand, the performance difference between QCP and OQCP decreases when imbalance σ_0 decreases (impact of amplitude weights is smaller) or number of antennas M increases (fast signal variation becomes smaller).

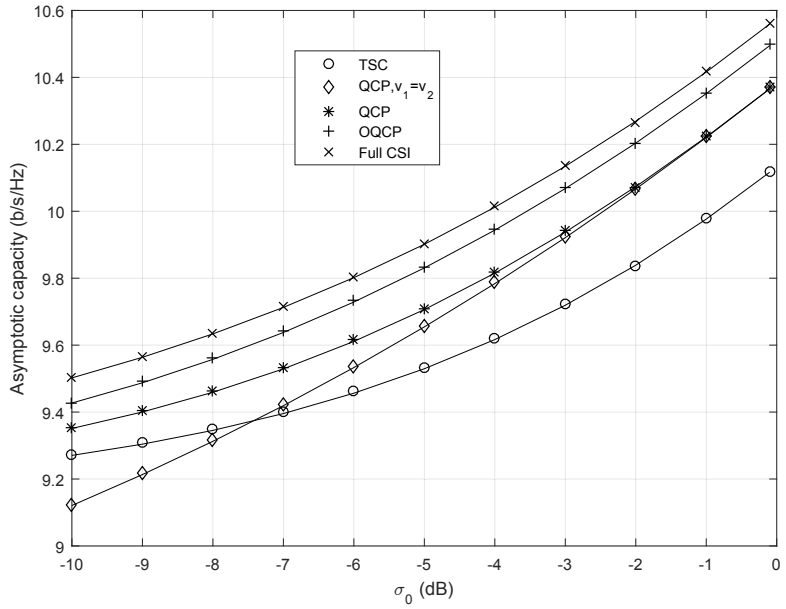

Figure 4.4. Asymptotic capacity as a function of σ_0 when $M = 1$, $N_w = 3$, $N_\mathrm{u} = 2$ and $\bar{\gamma}_1 = 30$dB. Solid curves refer to the analytical results and markers refer to the numerical results.

4.5.4 Bit error rate

The impact of imbalance on the BER of the studied schemes is shown in Figure 4.5 where average BER results are presented in terms of power imbalance assuming $\bar{\gamma}_1 = 15$ dB and $N_w = 3$. The analytical BER results in (4.29), (4.30), and (4.31) are depicted with solid curves and they fit well with the simulated BER results depicted with markers. We observe from Figure 4.5 that unlike in the case of SNR gain and average capacity, the performance of QCP, when applying the SNR maximizing weights, falls behind the TSC performance after a power imbalance value of around 5 dB. On the other hand, QCP applying the asymptotic BER minimizing weights performs close to OQCP at large imbalance.

We present simulated BER results in Figure 4.6 for $M = 4$, $\bar{\gamma}_1 = 3$ dB, $N_w = 3$, and $N_u = 2$ to observe impacts of using a larger number of antennas in BSs. In contrast to the $M = 1$ case, QCP with SNR maximizing weights performs close to OQCP, particularly for large power imbalance. This shows the multiple antennas at least from the stronger group provide better diversity irrespective of value of imbalance.

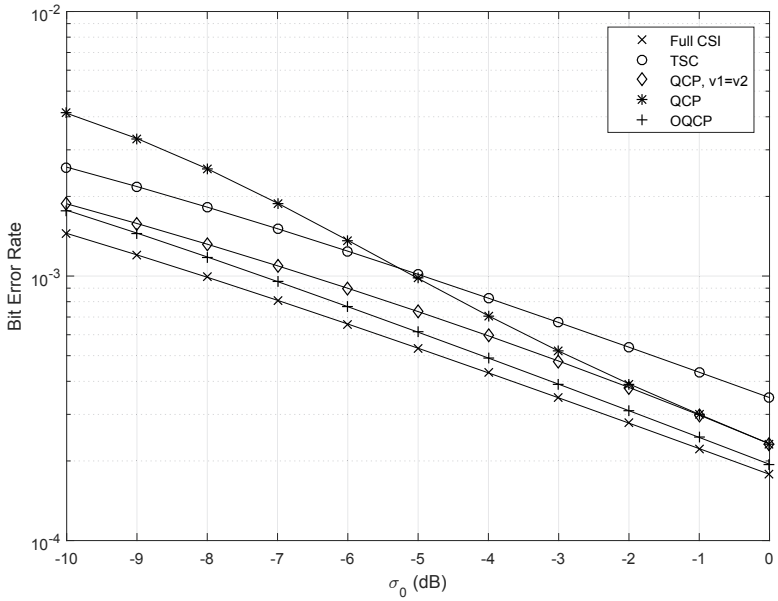

Figure 4.5. Average BER as a function of σ_0 for QCP, OQCP, TSC and full CSI schemes when $M = 1$ and $\bar{\gamma}_1 = 15$ dB. Solid curves refer to analytical results and markers refer to simulated results.

4.5.5 Impact of erroneous feedback

To observe the impact of erroneous feedback, Figure 4.7 presents simulated asymptotic capacity assuming errors on feedback bits and $M = 1$, $N_w = 3$ and $N_{\mathrm{u}} = 2$. Solid curves shows results without feedback bit error and dashed curves depicts results with a 20% bit error probability. Simulations are carried out assuming 3-bit Gray coding for the quantized phases and uniformly distributed bit errors that occur with the same probability for the short-term order and phase feedback bits used in the methods between antenna groups.

We observe that for large power imbalance, OQCP and TSC show the highest capacity loss (up to 8%) due to feedback errors. The loss for OQCP has smaller variation with respect to imbalance but the loss for TSC significantly increases when σ_0 decreases. For QCP, it is also observed that the capacity loss decreases when power imbalance increases irrespective of the possibility of exploiting long-term feedback.However, in case of large imbalance, QCP with long-term weights provides considerably smaller capacity loss than QCP with the equal weights. Furthermore, according to [PII] (Figure 11) we note that when more transmit antennas are utilized in BSs, relatively small decrement on capacity loss is observed for both QCP and OQCP when large power imbalance occurs.

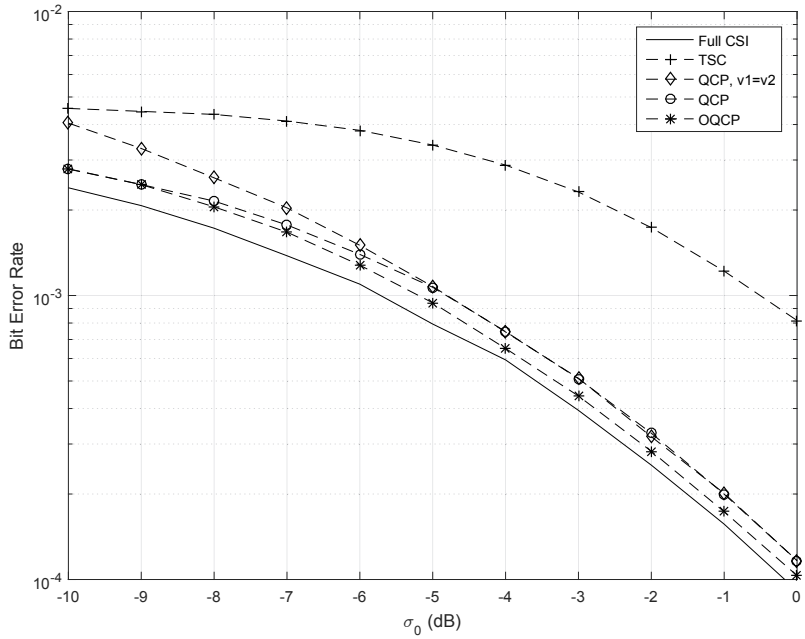

Figure 4.6. Simulated BER as a function of σ_0 for QCP, OQCP, TSC and full CSI schemes when $M = 4$ and $\bar{\gamma}_1 = 3$ dB.

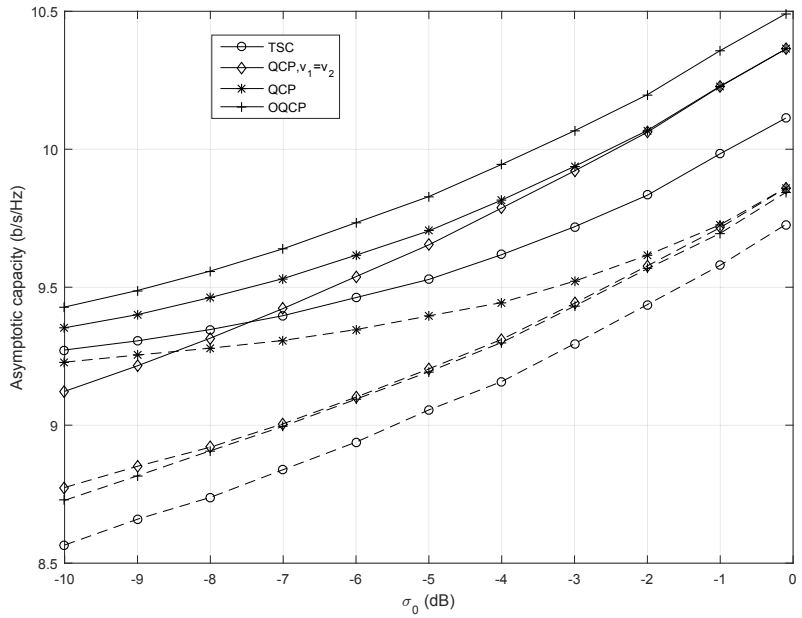

Figure 4.7. Asymptotic capacity as a function of σ_0 when $M = 1$ and $\bar{\gamma}_1 = 30$dB. Solid curves refer capacity results in the absence of feedback bit error and dashed curves refer capacity results with a 20% bit error probability.

5. Performance evaluations of CoMP for LTE-A system in dense urban scenarios

Besides theoretical analyses, performance gains of CoMP have been evaluated using field trials [9] and system simulations [13, 14]. Most of simulation studies have considered uniform 2D network layouts and empirical propagation models such as Okumura-Hata and Walfisch-Ikegami models with log-normal shadowing. In contrary, we have performed thorough simulation campaigns of CoMP transmission for conventional and heterogeneous urban LTE-A network deployments considering deterministic 3D propagation models. While [PIV] considered CoMP enhancements for selected cell-edge users in conventional LTE-A network, [PV], [PVI] and [PVII] focus on CoMP usage to relax wireless backhaul of LPNs deployed in HetNet. Furthermore, analytical outage capacity result considering Rician channel for serving BS and Rayleigh channel for rest of BSs in a given CoMP set has been presented in [PV].

Used channel model is explained first in Section 5.1. Then the validated analytical result for outage capacity is provided in Section 5.2. Sections 5.3 and 5.4 summarize results of the simulation campaigns when CoMP is applied to enhance links of cell-edge users and LPNs, respectively. Three case studies are simulated each with its own scenarios that will be explained in respective sections.

5.1 Channel model and SINR formulation

In general, average power $\bar{\gamma}_m$ of a channel from the m^{th} evolved NodeB (eNB) to a given target UE or LPN is determined based on average pathloss and shadow fading components. For accurate pathloss modeling, we use a computationally efficient dominant path ray tracing model implemented in the WinProp propagation tool [63]. Furthermore, we assume realistic simulation environment with 3D buildings and topography data

for simulation area and 3D antenna patterns. In Figure 5.1 pathloss results obtained for a BS deployed at a height of 25 m in the Meskel Square area of Addis Ababa, Ethiopia have been illustrated. Shadow fading is modeled using the classic log-normal distribution with a given standard deviation and decorrelation distance. While Rayleigh fast fading is considered for links without LOS connection, Rician model is used for links with LOS connection.

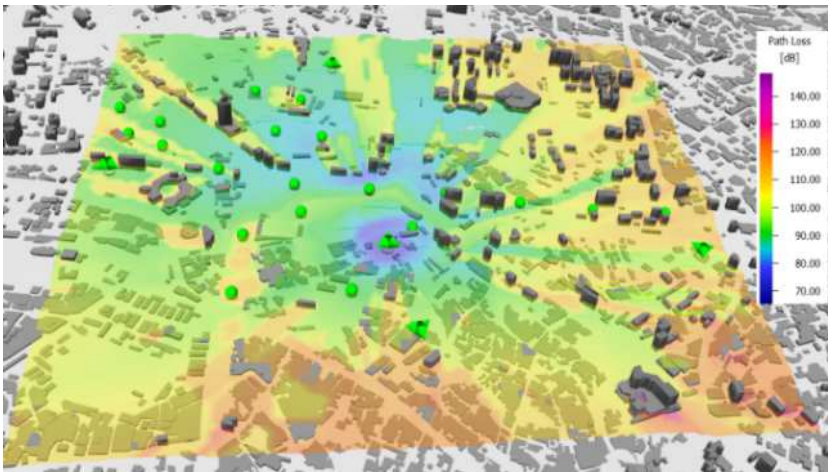

Figure 5.1. Example: 3D view of path loss map at prediction height of 1.5 m for a BS deployed at a height of 25 m in the Meskel Square area.

Let us consider the LTE network with L single-antenna eNBs serving UEs (and LPNs in HetNet). The instantaneous SINR in the absence of CoMP at reception can be expressed as

$$z_{\mathrm{nc}} = \frac{P_t \gamma_1}{P_t \sum_{m=2}^{L} \gamma_m + P_n}, \tag{5.1}$$

where γ_m is the received channel power at the UE/LPN from the m^{th} eNB. We assume that cell selection is made based on average received power $\bar{\gamma}_m$ and index 1 references the serving eNB. When we apply a joint transmission CoMP, some of the most interfering links are now exploited to enhance the link. Unless explicitly mentioned, QCP is assumed to be the applied CoMP technique in this chapter. For a CoMP set Q consisting of $\mathcal{Q}$ eNBs, the SINR in this case takes the form

$$z_{\mathrm{c}} = \frac{u P_t |\sqrt{\gamma_1} + \sum_{m \neq 1, m \in Q} \sqrt{\gamma_m} e^{j\theta_m}|^2}{P_t \sum_{m \notin Q} \gamma_m + P_n}, \tag{5.2}$$

where θ_m is uniformly distributed variable on the range $(-\pi/2^{N_m}, \pi/2^{N_m})$ and u is a parameter to determine whether full transmission power is applied in each eNB.

5.2 Analytical results for outage capacity

In [PV], we presented analytical expressions for outage probability for the non-CoMP and CoMP cases assuming Rician channel for serving eNB and Rayleigh channels for remaining eNBs. First, if CoMP is not applied, then outage probability attains the form [64]:

$$P_o^{\text{nc}} = 1 - \sum_{j\neq 1} D_m \Big[1 - \frac{\bar{\gamma}_m(K+1)Z_r}{\bar{\gamma}_1 + \bar{\gamma}_m(K+1)Z_r} \exp\left(\frac{-K\bar{\gamma}_1}{\bar{\gamma}_1 + \bar{\gamma}_m(K+1)Z_r}\right)\Big], \quad (5.3)$$

where Z_r is required SINR, K is the Rician factor and $D_m = \prod_{i\neq m} \bar{\gamma}_m/(\bar{\gamma}_m - \bar{\gamma}_i)$.

For the CoMP transmission with $\mathcal{Q} = 3$, the analysis in [PV] provides an approximate tight lower-bound outage probability expression of the form

$$P_o^{\text{c}} = 1 - \sum_{m\notin C} D_m \left(1 - \frac{\mathcal{M}^3}{2} \sum_{i=1}^{3} a_i (i+1)! \left(\frac{u\bar{\gamma}_m Z_r}{P_t + \mathcal{M} u \bar{\gamma}_m Z_r}\right)^{i+2}\right), \quad (5.4)$$

where $\mathcal{M} = 3/\mathbb{E}\{\eta_1\}$, $a_3 = 2\mathcal{M}^2(\mathcal{M}^2\mathbb{E}\{\eta_1^2\}/48 - 0.25)$, $a_2 = -8a_3/\mathcal{M}$, $a_1 = -\mathbb{E}\{\eta_1\}a_2/2 + 1$ and instantaneous power $\eta_1 = P_t|\sqrt{\gamma_1} + \sqrt{\gamma_2}e^{j\theta_2} + \sqrt{\gamma_3}e^{j\theta_3}|^2$. Expressions for the 1^{st} and 2^{nd} moments of η_1 can be computed analytically. We have

$$\begin{aligned}\mathbb{E}\{\eta_1\} =& P_t\Bigg(\bar{\gamma}_1 + \bar{\gamma}_2 + \bar{\gamma}_3 + \frac{\pi}{2}\sqrt{\frac{\bar{\gamma}_1}{K+1}} M(-1/2, 1; -K)\left[\sqrt{\bar{\gamma}_2}\mathcal{C}_2 + \sqrt{\bar{\gamma}_3}\mathcal{C}_3\right] \\ &+ \frac{\pi\sqrt{\bar{\gamma}_2\bar{\gamma}_3}\mathcal{C}_2\mathcal{C}_3}{2}\Bigg), \end{aligned} \quad (5.5)$$

where $M(\cdot,\cdot;\cdot)$ is the confluent hypergeometric function defined in [50, 13.2.1], and $\mathcal{C}_m = \mathbb{E}\{\cos\theta_m\} = \text{sinc}(\pi/N_m)$. Similarly we can find expression for $\mathbb{E}\{\eta_1^2\}$.

Figure 5.2 illustrates outage probability as a function of targeted capacity (i.e. $\log_2(1 + Z_r)$) for a UE/LPN deployed within a given 3 site 9 cell network [PV]. Results are obtained for $K = 3$ dB, $N_1 = N_2 = 3$ and average channel powers (in dB scale) of -70.6017, -90.9171, -87.5557, -80.8873, -98.5906, -100.6473, -76.5733, -92.9982, -96.1564 (results obtained using a dominant path model for a given location with respect to the 9 cells [PV]). Solid curves refer to analytical results and markers refer to numerical results. For benchmarking purpose, we also present results when full CSI is available at the transmitter side, the corresponding results depicted with dashed and dash-dotted curves in the figure. We can see that our results obtained from (5.4) fit well with the corresponding numerical results. The QCP based CoMP transmission considerably improves outage probability performance. For instance, compared to non-CoMP case,

4.37 b/s/Hz and 2.83 b/s/Hz better capacities are seen at the $50\%-$ile when each coordinating cell applies full ($u = 1$) and one third ($u = 1/3$) transmit power, respectively. Furthermore, QCP based CoMP with the few number of feedback bits performs close to the full CSI case.

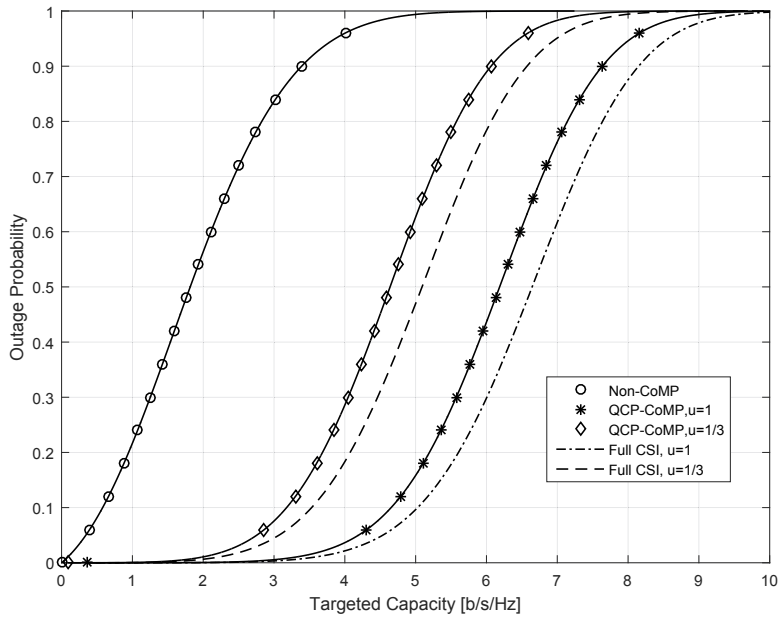

Figure 5.2. Outage probability as a function of required capacity. Solid curves refer to the analytical results; markers refer to the numerical results; and dashed and dash-dotted curves refer to the full CSI case.

5.3 QCP-CoMP gains in conventional LTE-A urban deployment

5.3.1 Network layout and assumptions

The simulation study in [PIV] considered downlink inter-site CoMP transmission for three single antenna macro eNBs deployed in Hanna Nasif area with an inter-site distance of approximately 500m, as depicted in Figure 5.3. Hanna Nassif is a densely populated urban ward in Dar es Salaam, Tanzania with an estimated population of 40000 people, living in a 1 km^2 land area. The simulation area shown in the figure includes around 3000 (mostly single story) buildings and is located on a terrain with a topographical difference of 19 m. LTE-A capable users are randomly dropped in the simulation area to be served with or without CoMP based on a given criterion.

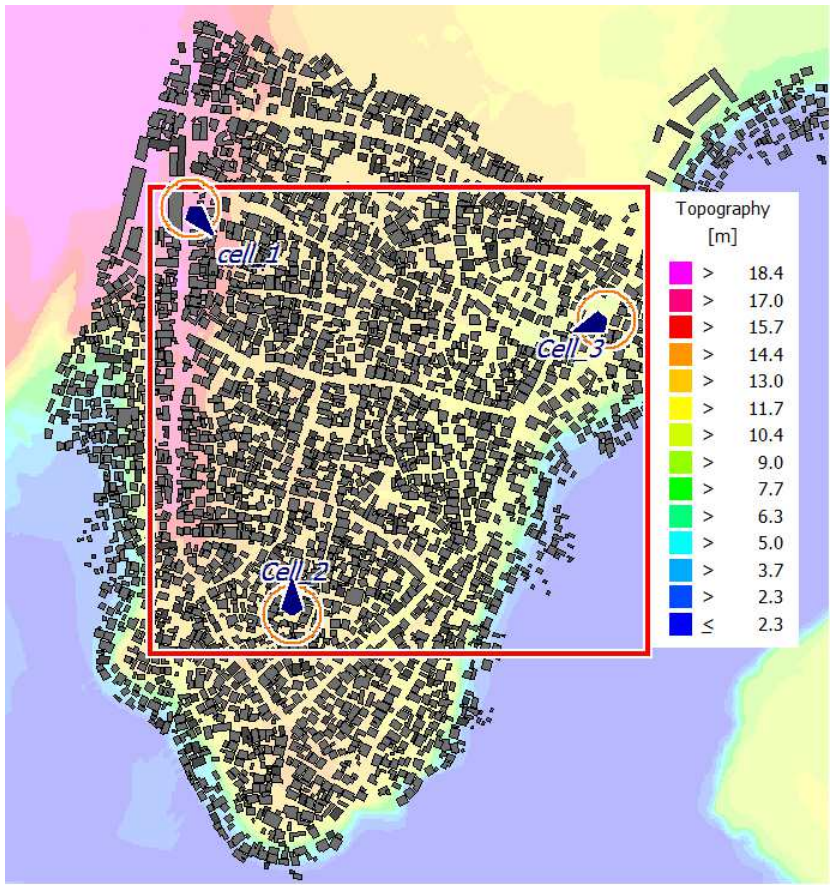

Figure 5.3. Macro cellular network layout in Hanna Nasif area.

CoMP criterion: CoMP UEs are selected based on the average difference between best received signal powers from Cell 1 and Cell 2, and Cell 1 and Cell 3. Thus, a given UE is CoMP UE if

$$\frac{|\bar{\gamma}_1 - \bar{\gamma}_2| + |\bar{\gamma}_1 - \bar{\gamma}_3|}{2} \leqslant T, \tag{5.6}$$

where T is target threshold in dB and values of received powers are also in dB scale. All cells are involved in the CoMP coordination.

QCP CoMP method: Assuming the branch with best received power as a reference, CoMP UE select appropriate phase weights for remaining eNBs and send corresponding feedbacks to the eNBs.

System simulation campaign is performed to investigate network performance. Parameters and assumptions that are set based on commonly-used 3GPP guidelines [13]. Assumptions used for the simulation are listed in Table 5.1.

Table 5.1. Basic simulation parameters and assumptions

Parameter	**Values/Assumptions**		
Air Interface	LTE FDD		
Carrier Frequency	2000MHz		
Simulation	Radio propagation modeling (WinProp) Static sytem level simulation (Matlab) 5m resolution; 1.5m predition height		
CoMP	QCP with $N_w = 3$ feedback bits, $\mathcal{Q} = 3$		
Spectral Efficiency	$B_{\text{eff}} = 0.62$, $z_{\text{eff}} = 1.8$, $z_{\min} = -10$dB,$S_{\max} = 4.4$b/s/Hz		
Macro (eNB) Parameters			
Macro Cells	Cell 1	Cell 2	Cell 3
Transmit power	46 dBm		
Antenna Height	15 m	20 m	25 m
Antenna Patterns	Kathrein 741984		
Azimuths	140	0	250
Intersite Distance	Approximately 500m		
UE Parameters			
Noise Figure/Mean UE Number	9 dB/20 UE per macrocell		
Antenna Configuration	1x2		
Buildings and Fading Characterstics			
Buildings	Building of variable dimensions, height 3-6 m Building penetration loss: 10dB		
Fading	Shadow fading: Gaussian (0 dB mean, $\sigma_s = 8$ dB), 50 m decorrelation distance Fast fading: Zero mean complex Gaussian		

5.3.2 Performance results

The number of CoMP UEs as a fraction of the all UEs for different CoMP thresholds is shown in Table 5.2. We see that relaxation of the CoMP criterion (by increasing the CoMP threshold) results in a larger number of UEs that are able to exploit CoMP transmission, including UEs with large average power imbalance.

Table 5.2. Percentage of CoMP UEs for different thresholds

	Threshold T [dB]			
	1	3	6	10
CoMP UE Percentage	0.5%	2.5%	15%	36%

The cumulative distribution function (CDF) of SNR gain of QCP over non-QCP UEs at different thresholds is illustrated in Figure 5.4 assuming full transmit power at the macrocells. As expected, the best SNR gain

performance is achieved for the smallest threshold, thus for the smallest average power imbalance, as also observed in the analysis of Section 4. On the other hand, we find that the best performance corresponds to the

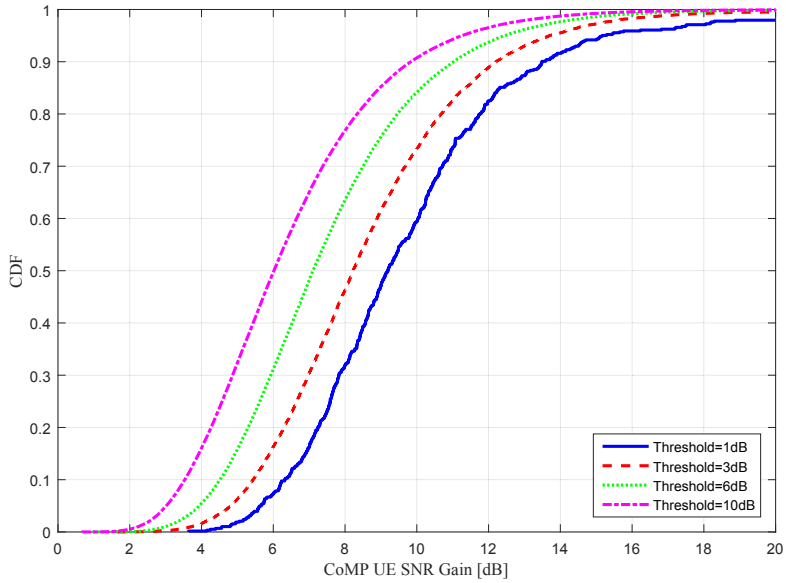

Figure 5.4. Distribution of SNR gain due QCP for CoMP UEs when $u = 1$.

largest threshold if all UEs are considered as can be seen in Figure 5.5. This is because the higher the threshold the larger the number of UEs able to leverage and benefit from CoMP (as noted in Table 5.2). For small CoMP thresholds ($\leqslant 3$ dB), the SINR performance improvement relative to non-CoMP case is negligible due to smaller number of CoMP UEs although the SINR performance of those few lucky CoMP UEs are considerably improved. Furthermore, we note that applying full $(u = 1)$ instead of one third $(u = 1/3)$ transmit power in eNB has insignificant impact on overall SINR performance (see Figure 3 in [PIV]). This is mainly due to the fact that most of the SINR gain is achieved from interference mitigation rather than from improvements in power of the desired signal.

The CDF of the spectral efficiency for all UEs, mapped from the simulated SINR, is shown in Figure 5.6 when $u = 1/3$. The large threshold ($\geqslant 6$) dB provides highest overall spectral efficiency gains from CoMP. However, when spectral efficiency gain of an individual CoMP UE is considered (see Figure 5.7), the highest spectral efficiency gains occur when UE is experiencing small power imbalance (low CoMP threshold). Insignificant efficiency gain for CoMP UEs is also seen when eNBs apply full transmission power (see Figure 8 in [PIV]). This might provide a

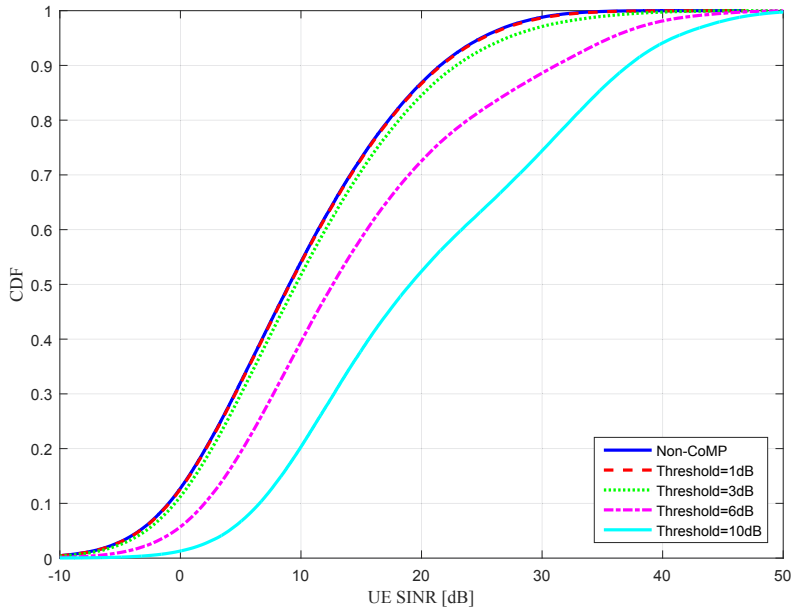

Figure 5.5. SINR distribution for all UEs when $u = 1/3$.

room for efficient energy usage as BS transmit power is one of influential variables in power models developed to study power consumption of CoMP systems [65].

5.4 QCP-CoMP to relax self-backhauling bottlenecks in HetNets

This section summarizes studies of [PV, PVI, PVII], investigating the potential use of CoMP for enhancing wireless backhaul capacity in HetNets with LPNs. Wireless backhauling solution for LPNs is desirable for outdoor deployment scenarios that are strongly constrained by backhaul cost and demand for high deployment flexibility. Examples of such scenarios include densely populated areas, semi-permanent networks (e.g., for open air festivals), and spontaneous or rapid network deployment (e.g., public safety communications) [66, 67].

5.4.1 Self-backhauled LPN and capacity bottleneck

The backhaul of LPNs can be fixed or wireless links and we call it self-backhauling when the backhaul is wireless and via the existing macro RAN. Self-backhauling is an attractive backhauling solution for certain LPN deployment scenarios. In Figure 5.8 we provide a simple illustra-

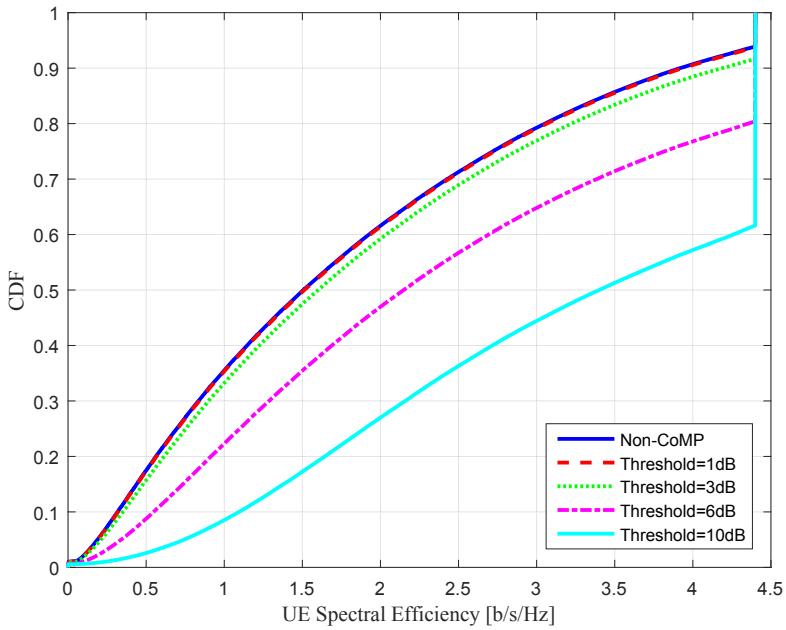

Figure 5.6. Spectral efficiency distribution for all UEs when $u = 1/3$.

tion to describe the difference between conventional fixed-wireless backhauling and self-backhauling for LPNs. Conventional wireless backhauling for LPNs relies on dedicated P2P or P2MP fixed-wireless technologies (e.g. millimeter wave radios) with stringent LOS requirements between the LPN and the wireless hub which may be collocated with a macro site (see Figure 5.8a) [68]. By contrast, in Fig. 5.8b self-backhauling is provided via the macro RAN for LPNs deployed within the coverage area of a particular eNB, with the macrocell resources being shared by other LPNs and/or macro UE located within the same coverage area.

The LPN self-backhauling approach provides a number of benefits compared to the conventional fixed-wireless backhauling. These include: cost savings by leveraging existing macrocell site infrastructure; backhauling in NLOS conditions using legacy cellular spectrum bands (typically below 3.5 GHz), use of emerging lightly licensed bands (e.g. TV white space), and possible joint radio resource management of backhaul and access links [69]. These self-backhauling benefits have motivated the development of the relaying concept introduced in LTE-A [70]. The self-backhauling approach can be extended to include all types of LPNs (beyond relays) providing flexibility in selection of RATs, operating spectrum band, and radio resource management strategies [71–73].

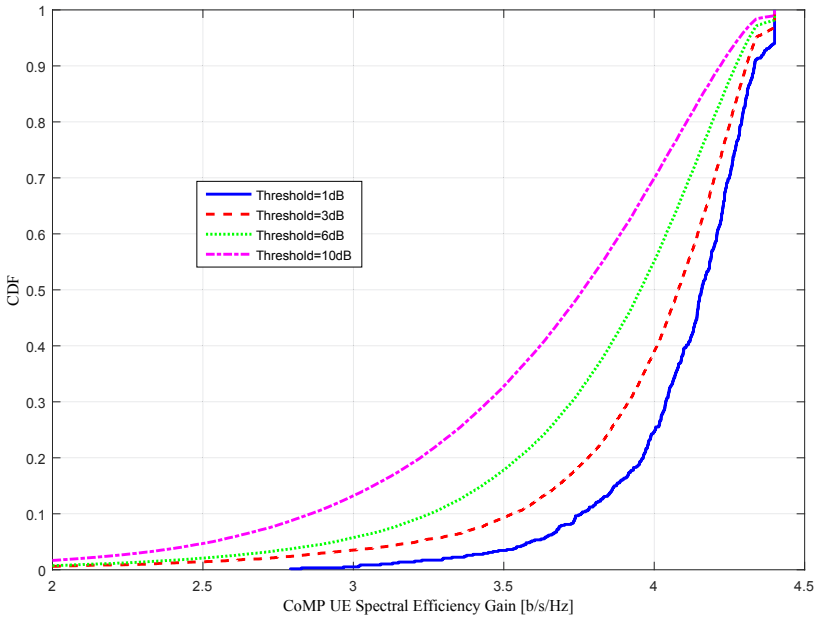

Figure 5.7. Spectral efficiency distribution for all UEs when $u = 1/3$.

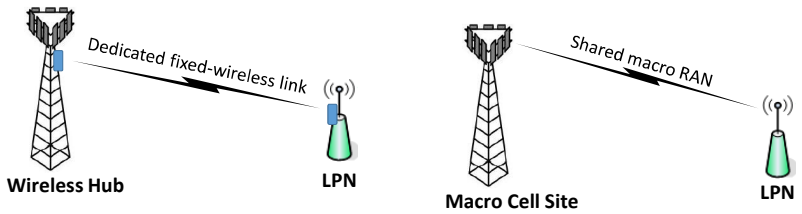

(a) Fixed-wireless backhauling (b) Self-backhauling

Figure 5.8. Backhauling of LPN using (a) fixed-wireless links and (b) self-backhauling via macro RAN.

The self-backhauling with the use of macro resources in the backhaul is a key factor while utilizing the benefits of cost-effectiveness and flexibility in LPN deployment. However, the reuse of the macro resources usually results in a backhaul capacity bottleneck, whereby, the potential aggregate capacity of LPN access exceeds the achievable wireless backhaul capacity. This capacity bottleneck will consequently limit peak achievable throughputs for the UE served by the LPN.

Site planning has been proposed to enhance backhaul capacity for relay deployment in [74–76] though authors assume a set of spatially distributed good candidate sites which is practically difficult to achieve due to the challenge of site acquisition. Higher order modulations (256 quadrature amplitude modulation, or higher) and MIMO configurations

have been considered in [73] to improve the backhaul capacity, yet to be effective such solutions require proximity to macrocell center and rich scattering environments in order to achieve their full potential. Furthermore, some resource sharing algorithms among LPNs based on their load and other factors has been suggested in [69, 77].

To relax the capacity bottleneck, we have investigated CoMP transmission applied at the backhaul as depicted in Figure 5.9. In the non-CoMP case, the LPN backhaul is served only by its best eNB, while the signals of the adjacent macrocells appear as interference. On the other hand, in the CoMP case, the self-backhauling of the LPN is provided jointly by all the coordinating macrocells.

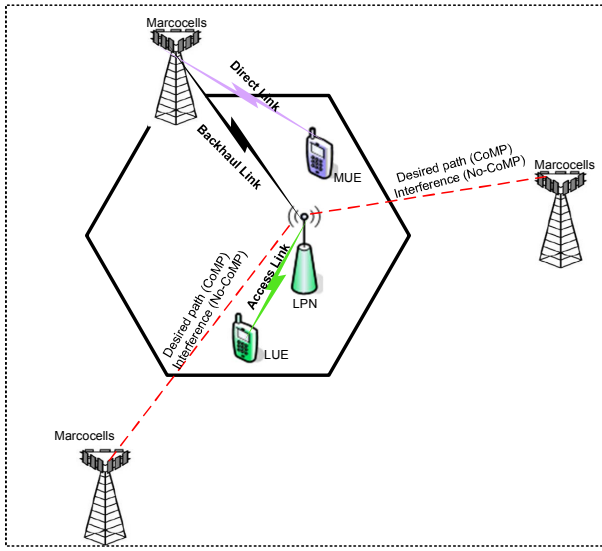

Figure 5.9. System illustration for LPN deployment. LUE and MUE refer to UE associated to LPN and macrocell, respectively.

5.4.2 LTE-A relay deployment

Deployment scenario and assumptions

We consider three tri-sector macro eNBs and three cell-edge RNs in the Hanna Nasif simulation area as illustrated in Figure 5.10. The label SxCy in Figure 5.10 is used to refer to cell (or sector) y of tri-sectored macro site x. We note that the LPN in Figure 5.10 refers to an LTE-A RN. Furthermore, we deliberately increase the number of macrocell coordination scenarios by placing the 3 RNs at the edges of three adjacent cells, such that, each RN is served by unique cell of a different site from the other

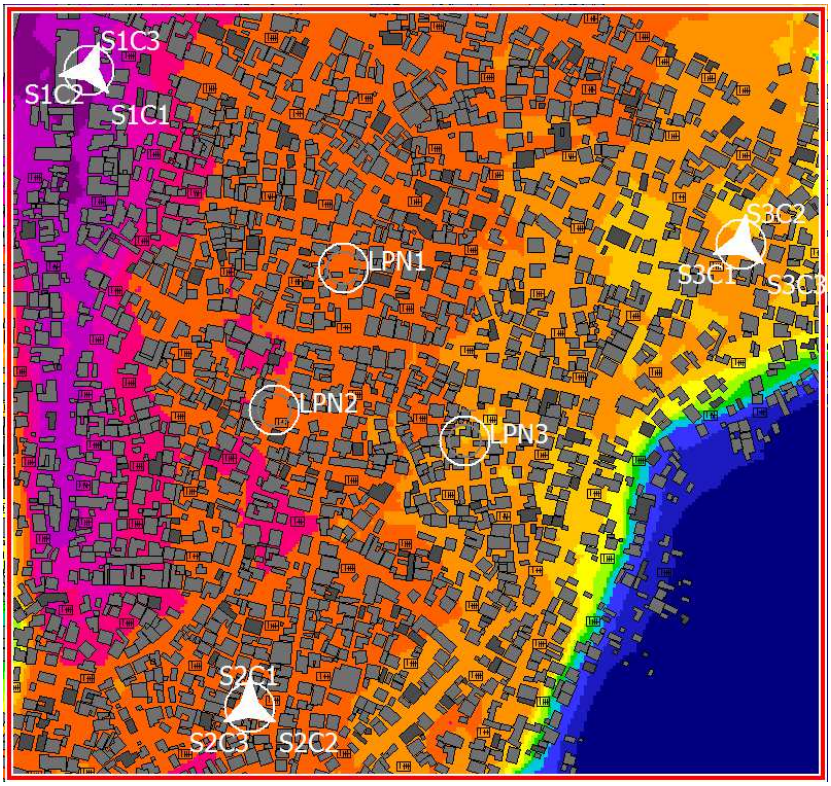

Figure 5.10. Deployment scenario for the CoMP-enhanced-relay-based HetNet.

2. To be specific using Figure 5.10, the deployment is such that S1C1 is donor cell for LPN1 (RN1); S2C1 is donor cell for LPN2 (RN2); and S3C1 is donor cell for LPN3 (RN3). We consider randomly located UEs in the simulation area.

Resource scheduling

In typical FDD LTE-A Type 1 inband relay scenarios, the RN, MUEs and LUEs are served on a common frequency band [70]. Time-domain half-duplexing is used to isolate backhaul and access link transmissions, with the RN continuously switching between the relay and access links to avoid self-interference, as illustrated in Figure 5.11. Note that parameter τ_r denotes time ratio allocated to the backhaul link.

When CoMP is serving the relay link during backhaul subframes, PRBs orthogonal in frequency domain are applied by eNBs to serve the RNs, and the resources are scheduled based on the classical round robin (RR) resource partitioning strategy that divide resources equally irrespective of CSI. In the access link subframes, we also assume that eNBs allocate their PRBs among their MUEs using the RR algorithm. At the RNs, it should

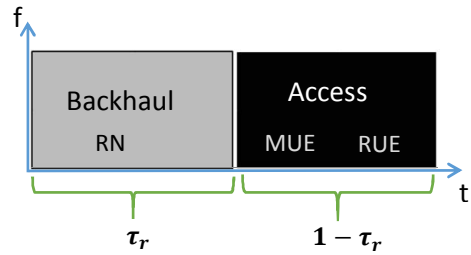

Figure 5.11. Resource allocation among RN backhaul, macro and relay users.

be noted that LUEs are not served during the backhaul subframes. We initially apply at each RN the classical RR scheduling that divides PRBs equally among LUEs. If backhaul becomes a bottleneck, which is mostly the case as will be noted from achieved result, the initially allocated resources are redistributed among the LUEs using max-min fair scheduling which priorities LUEs with lower throughputs [78]. We note that the practical scheduling implementations are mostly vendor-specific [2] and advanced CSI-based scheduling methods, such as, proportional fair can be applied to achieve better performance.

In simulation, we include the time share τ of each link in the throughput equation (2.12) to average over an LTE frame length:

$$\mathcal{T} = \tau \cdot N_{\text{PRB}} \cdot B_{\text{PRB}} \cdot \mathcal{S}, \tag{5.7}$$

where $\tau = \tau_r$ for relay link and $\tau = 1 - \tau_r$ for access links. We can select value τ_r that provides the optimal end-to-end (e2e) throughput which is achieved when the backhaul throughput is equal to the aggregate LUE access throughput. In practical LTE network, downlink backhaul radio resources are achieved by allocating RNs up to six multicast-broadcast single frequency network subframes (frame numbers 0, 1, 2, 3, 6, 7, 8) out of the 10 subframes (each of 1 ms duration) specified in the 3GPP Release 8 LTE frame structure [2]. Thus τ_r can take granular values such that

$$\tau_r \in \{0.1, 0.2, 0.3, 0.4, 0.5, 0.6\}.$$

If the τ_r that provides the optimal e2e throughput is greater than 0.6, then backhaul is a bottleneck, which is the most usual case. Our study focus on the CoMP benefit considering static allocation of 60% (maximum) or 30% of the subframes for the backhaul.

Performance results

System-level simulations are performed to investigate network performance for CoMP and non-CoMP scenarios on the RN backhaul link.

Simulation parameters and assumptions that are based on 3GPP guideline [13], see Table 5.3.

Table 5.3. Simulation parameters and assumptions for RN based HetNet

Parameter	**Values/Assumptions**		
Air Interface	LTE FDD		
Carrier Frequency/Bandwidth	2110MHz/10MHZ		
Simulation	Radio propagation modeling (WinProp) Static sytem level simulation (Matlab) 5m resolution 1.5m UE & 5m RN predition height		
CoMP	QCP with u=1, N=3 feedback bits, and $\mathcal{Q} = 3$		
Spectral efficiency	$B_{\text{eff}} = 0.62$, $z_{\text{eff}} = 1.8$, $z_{\text{min}} = -10$dB, $S_{\text{max}} = 4.4$b/s/Hz		
Macro (DeNB/eNB) Parameters			
Macro Sites	Site 1	Site 2	Site 3
Transmit power per antenna	46 dBm		
Antenna Height	18 m	20 m	25 m
Antenna Patterns	Kathrein 741984		
Sector Azimuths	20, 140, 260	0, 120, 240	10, 130, 250
Intersite Distance	Approximately 500m		
RN Parameters			
Transmit Power/Antenna Gain/Noise Figure	30 dBm/5 dBi/5 dB		
Deployment Height	5 m		
RN Locations	250 m from DeNB, 140 m inter-RN distance		
Antenna Configuration	1x2		
UE (LUE and MUE) Parameters			
Noise Figure	9 dB		
Antenna Configuration	1x2		
Mean UE Number	15 UE per macrocell		
UE Mobility	Mobility off 50% UEs dropped randomly in whole area 50% UEs cluster-dropped in 40m radius of RNs		
Buildings and Fading Characterstics			
Buildings	Building of variable dimensions, height 3-6 m Building penetration loss: 10dB		
Fading	Shadow fading: Dominant Path Model (WinProp) Fast fading: Rician fading (RN-DeNB, K=3 dB) and Rayleigh fading (Other links)		

The CDF of the backhaul and access throughput considering all RNs is illustrated in Figure 5.12. The value of τ_r is set to the maximum 0.6 for both CoMP and non-CoMP cases. We see that QCP-CoMP significantly improves the backhaul throughput (e2e throughput) and diminishes the gap between the backhaul and access.

Contribution of CoMP-enhanced backhaul on the LUE throughput is illustrated using a bar plot in Figure 5.13. The plot shows CoMP gains

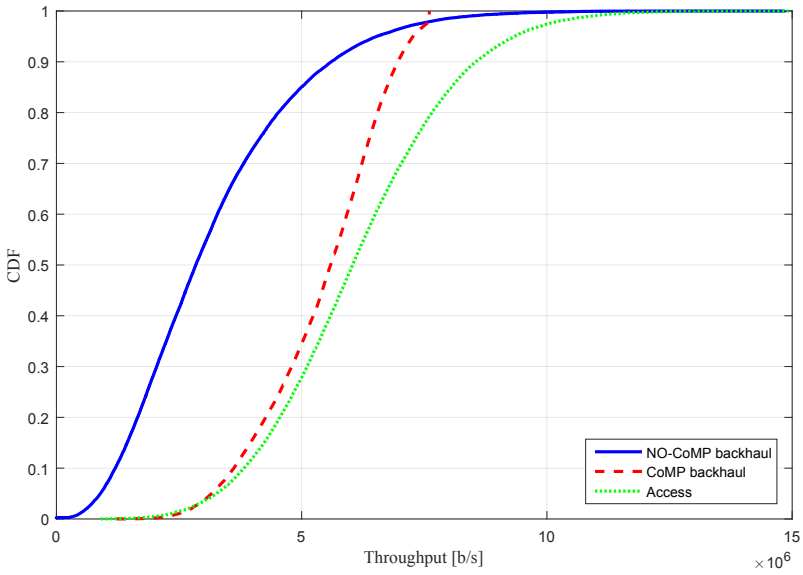

Figure 5.12. CDF of backhaul and access throughput. Solid curve refers to results for non-CoMP backhaul whereas dashed and dotted curves refer to results for CoMP backhaul and access, respectively.

over non-CoMP scenario when $\tau_r = 0.6$ and $\tau_r = 0.3$. We see that the applied CoMP scheme for both $\tau_r = 0.6$ and $\tau_r = 0.3$ significantly improves all the 10%-ile, 50%-ile and 90%-ile LUE throughputs. Unlike to $\tau_r = 0.6$ case, the scheme helps more the 10%-ile and 50%-ile when $\tau_r = 0.3$. Furthermore, the plot shows throughput gains of CoMP when $\tau_r = 0.3$ over non-CoMP case when $\tau_r = 0.6$. We note that there are still gains at 10%-ile and 50%-ile although loss is experienced at 90%-ile. Note that the reduction in τ_r allows for more time resources to be allocated for MUEs thus enhancing MUE throughput performance.

Performance impact of CoMP transmission over all UEs (both LUEs and MUEs) is illustrated in Figure 5.14. We see that CoMP delivers 10%-ile, 50%-ile and 90%-ile percentage gains of 85.96%, 56.98%, and 0.15% when $\tau_r = 0.3$, respectively. The percentage gain values are 8.48%, 43.83%, and 33.59% when $\tau_r = 0.6$. Note that CoMP improvements are more significant for the lower percentile throughput when $\tau_r = 0.3$ unlike the case when $\tau_r = 0.6$ where improvements are more to the higher percentile throughputs. If we compare CoMP with $\tau_r = 0.3$ and non-CoMP with $\tau_r = 0.6$, it is noted that CoMP with $\tau_r = 0.3$ provides 81.89%, 26.38%, and 24.07% 10%-ile, 50%-ile, and 90%-ile percentage gains, respectively, relative to the case of non-CoMP with $\tau_r = 0.6$.

To demonstrate impact of CoMP on the consistency of UE throughput

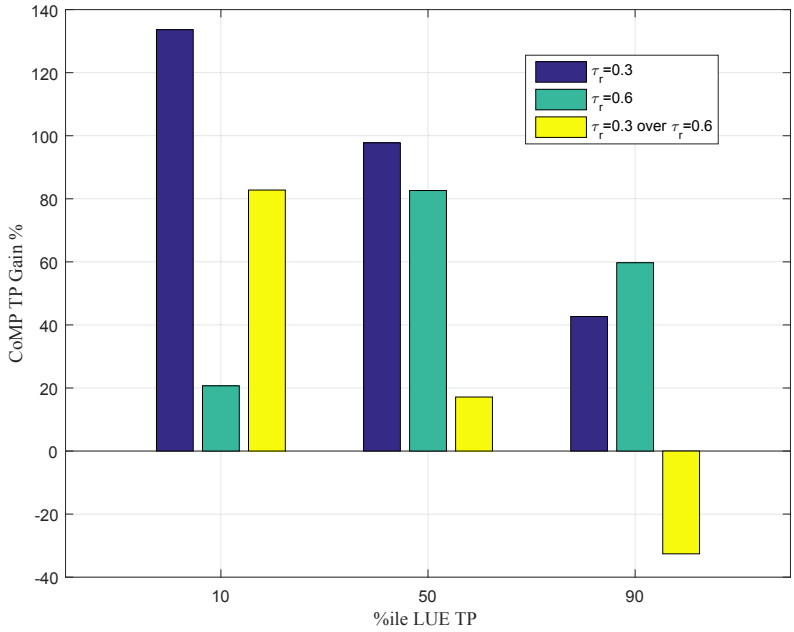

Figure 5.13. CoMP gain in terms of LUE 10%-ile, 50%-ile, and 90%-ile throughput when $\tau_r = 0.6$ and $\tau_r = 0.3$.

experience, we also present in Figure 5.15 CDF of fairness index defined as [79]

$$\text{FI} = \frac{\left[\sum_{i=1}^{N_{\text{ue}}} \mathcal{T}_i\right]^2}{N_{\text{ue}} \sum_{i=1}^{N_{\text{ue}}} \mathcal{T}_i^2}, \tag{5.8}$$

where N_{ue} is total number of UEs. The figure clearly shows that CoMP provides more consistent user experiences for both $\tau_r = 0.3$ and $\tau_r = 0.6$.

Assuming 3-bit Gray coding and uniformly distributed feedback bit errors, the negative impact of feedback errors on the CoMP throughput gain of LUEs is illustrated in Figure 5.16. We observe that large feedback bit-error probability can considerably diminish the CoMP benefit. The gain reduction at 10%-ile LUE throughput due to feedback bit errors is considerably higher when $\tau_r = 0.3$. On the other hand, the performance reduction due to feedback error when $\tau_r = 0.3$ and $\tau_r = 0.6$ is almost the same at 50%-ile.

5.4.3 Self-backhauled LTE-U LPN

Background on LTE-U LPNs

Operators usually employ co-channel deployment of LPNs whereby the LPNs utilize the same licensed spectrum bands as the macro cells for

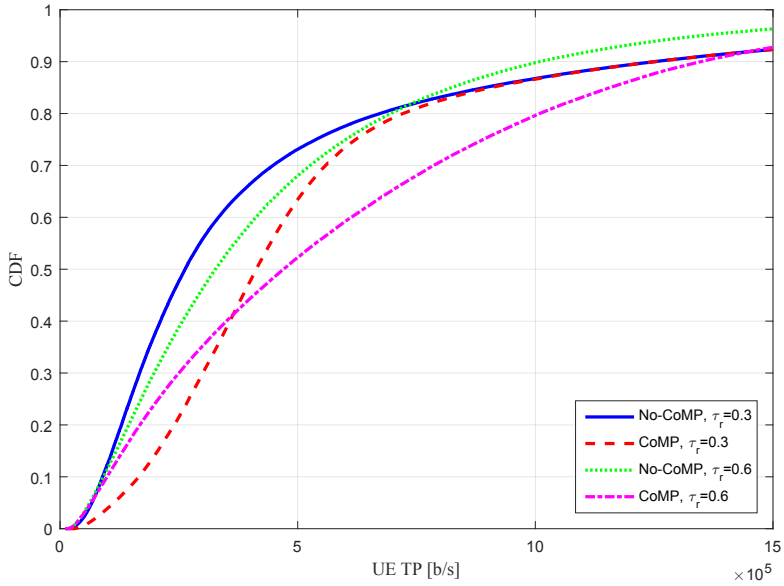

Figure 5.14. CDF of all UE throughput. Solid and dashed curves refer to results for non-CoMP and CoMP cases, respectively, when $\tau_r = 0.3$ whereas dotted and dash-dotted curves refer to non-CoMP and CoMP cases, respectively, when $\tau_r = 0.6$.

increased frequency reuse efficiency. However, this approach introduces the need to manage the interference and/or optimize resource allocation between the LPNs and the umbrella macro cellular layer [80]. Recently, the operation of LTE RANs in the unlicensed bands has been considered. This is commonly referred to as LTE-U or LTE License Assisted Access (LAA), and it has been subject of increased interest in research, industry and standardization, as it is viewed as one of the potential approaches for making available further spectrum for mobile radios towards 5G [81–83]. In the study in [PVII] we build on this growing interest by considering the opportunity of leveraging the license-exempt 5 MHz band for LTE-U LPNs serving dense urban hotspots. Specifically, consider the LPN in Figure 5.9 as self-backhauled out-of-band LTE-U LPN. To that end, we have investigated the HetNet when CoMP (and also carrier aggregation) is applied at the backhaul to relax the capacity bottleneck. Here we briefly summarize the achieved results.

Deployment scenario and simulation assumptions

We have used Meskel Square in Addis Ababa, Ethiopia as a simulation study area that exemplifies an urban scenario with dense hotspots. It covers an area of 1.25 km X 1.65 km including buildings of various heights

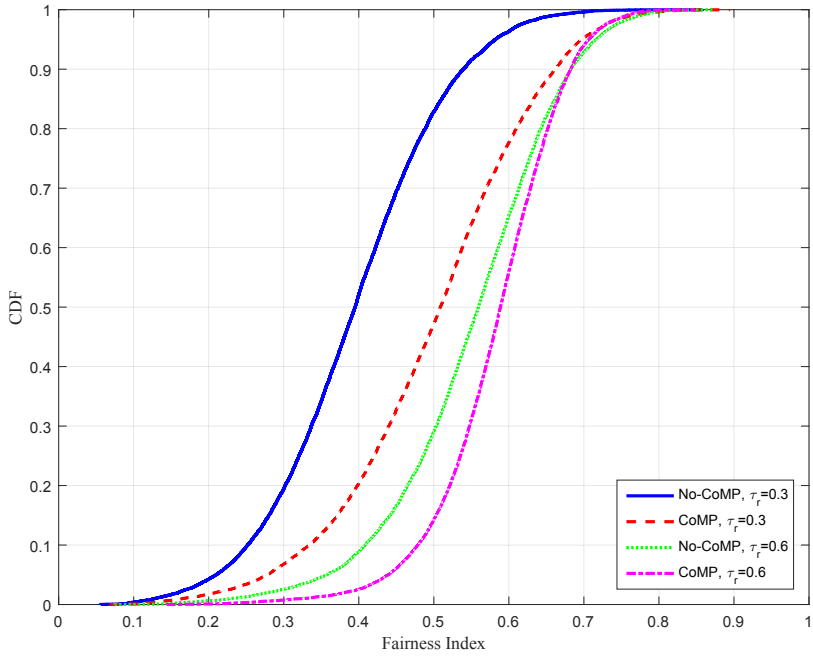

Figure 5.15. CDF of fairness index. Solid and dashed curves refer to results for non-CoMP and CoMP cases, respectively, when $\tau_r = 0.3$ whereas dotted and dash-dotted curves refer to results for non-CoMP and CoMP cases, respectively, when $\tau_r = 0.6$.

up to 79 m on a terrain with topography range of 2000-3000m (see Figure 5.17). In addition to Meskel Square, the study area includes the national stadium, exhibition center, hotel garden, as well as busy streets with light rail stations as major high user density spots. Five tri-sector macro sites are deployed in the simulation area with locations selected by approximations obtained from Opencellid [84]. Four of the fifteen macrocells are not activated for the simulation area due to their azimuths covering areas outside the study area. Under this macro umbrella, twenty outdoor LPNs are deployed at the aforementioned hotspot areas with a distance of at least 100m between the neighboring LPNs. In Figure 5.17, macro sites and LPNs are identified with green and red markers, respectively.

We consider CoMP transmission for LPNs meeting the condition given in (5.6). System-level simulation campaign is performed for assumptions and parameter values provided in Table 5.4 [85].

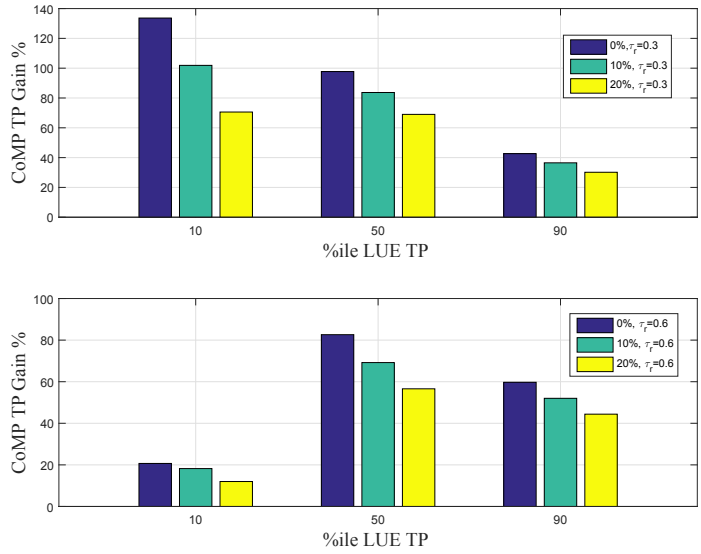

Figure 5.16. CoMP gain in terms of LUE 10%-ile, 50%-ile, and 90%-ile throughput for 0%, 10% and 20% bit error probability cases when $\tau_r = 0.6$ and $\tau_r = 0.3$.

Performance results

We note large throughput gap between the backhaul and access links of the LPNs as depicted in Figure 5.18. We see from the figure that CoMP transmission applied to 70% of the LPNs provides a small gap reduction relative to the large gap. Yet, this CoMP enhancement of the backhaul results in considerable throughput improvement for the LUEs as can be seen in Figure 5.19.

The CoMP gives 95.52%, 129.25%, and 63.74% LUE throughput gain at 10%-ile, 50%-ile, and 90%-ile, respectively.

The throughput gap can be further reduced by making more bands available for the backhaul, for instance through carrier aggregation as investigated in [PVII]. Combination of CoMP and carrier aggregation can full address the backhaul bottleneck challenge.

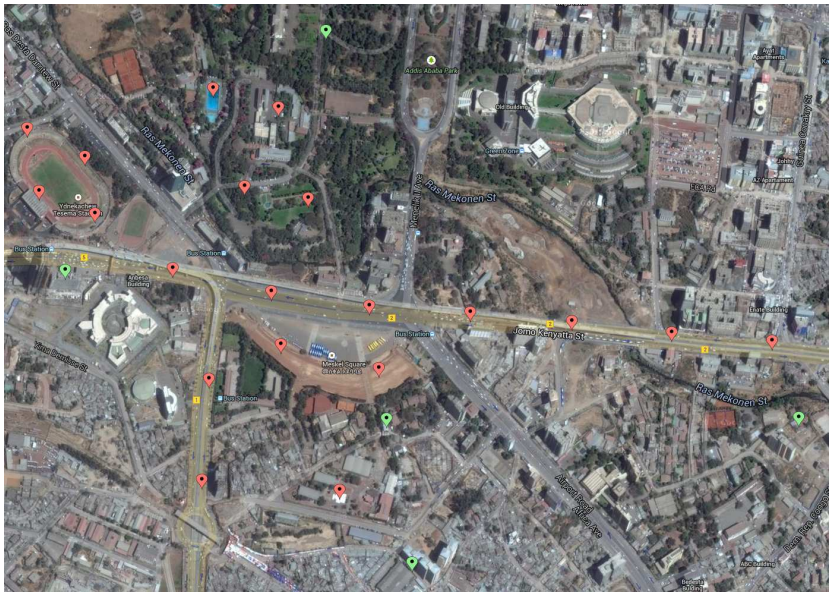

Figure 5.17. Satellite view of the Meskel Square surrounding.

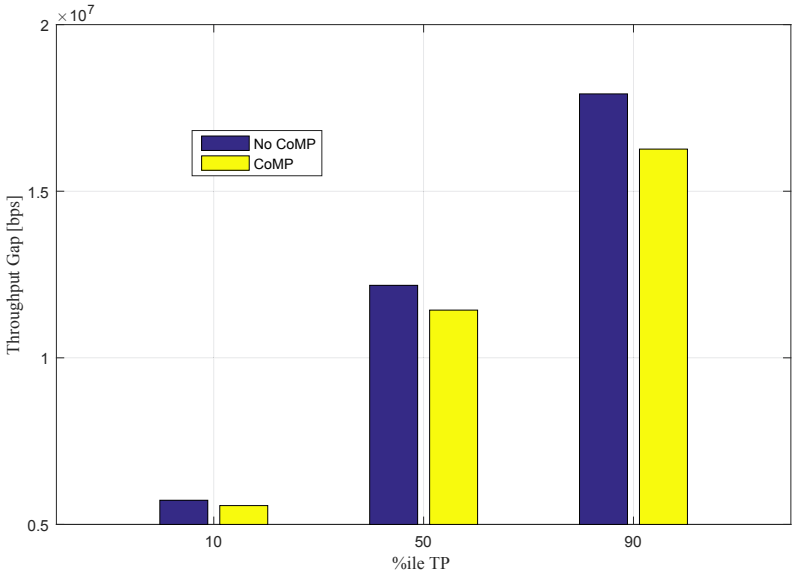

Figure 5.18. Average throughput gap between backhaul and access links of LPNs.

Table 5.4. Simulation parameters and assumptions for LTE-U based HetNet

Parameter	Values/Assumptions
Air interface	LTE FDD
Deployment Scenario	Outdoor LTE-U LPNs deployment; separate frequency between macro cells and LPNs
Carrier Freq./Bandwidth	2000 MHz/ 10 MHz for macrocell; 5000 MHz/5 MHz for LPN
Simulation	Radio propagation modeling (WinProp) [21]; System-level simulation (Matlab); 5 m resolution
CoMP scheme	QCP with N=3, C=3, and 6 dB CoMP threshold
Spectral efficiency	-10 dB, 0.72, 1.8, 4.4
Macro parameters	
Transmit power	46 dBm
Antenna height	25 m
Antenna pattern	Kathrein 742215 for 2000 MHz; Same pattern with K. 742215 for 5000 MHz
LPN parameter	
LPN number	20 LPNs: 2 for the Meskel Square, 4 for the stadium, 4 for the hotel garden, 1 for exhibition center and remaining 9 for the busy streeets
Location/height	Deployed in hotspot locations at height of 10 m
Antenna/transmit power	Omni antenna, 30 dBm transmit power
Backhaul reception	0 dBi Antenna gain, 5 dB noise figure, and 1x2 SIMO antenna configuration
UE parameters	
UE number/height	135 UEs in the service area/1.5 m UE height;
UE location	40% UEs dropped in whole area (both indoor and outdoor); 60% UEs cluster-dropped within 50 m radius of LPNs
UE reception	0 dBi antenna gain; 9 dB noise figure; 1x2 SIMO config.
Building, fading, and scheduling assumptions	
Buildings	Heights 3 to 79 m; 20 dB penetration loss
Shadow fading	Log-normal with standard deviation of 6 dB for direct and access links 4 dB for backhaul link
Fast fading	Rayleigh for direct and access links Rician with K=5 dB for backhaul link
Cell association	reference symbol received power based with 3 dB cell selection bias for LPNs
Scheduling	Frequency domain RR scheduling for macro cells and LPNs; Number of PRBs for LPN backhaul is based on number of associated LUEs; In case of CoMP, the minimum allocated number of PRBs is used by coordinating eNBs.

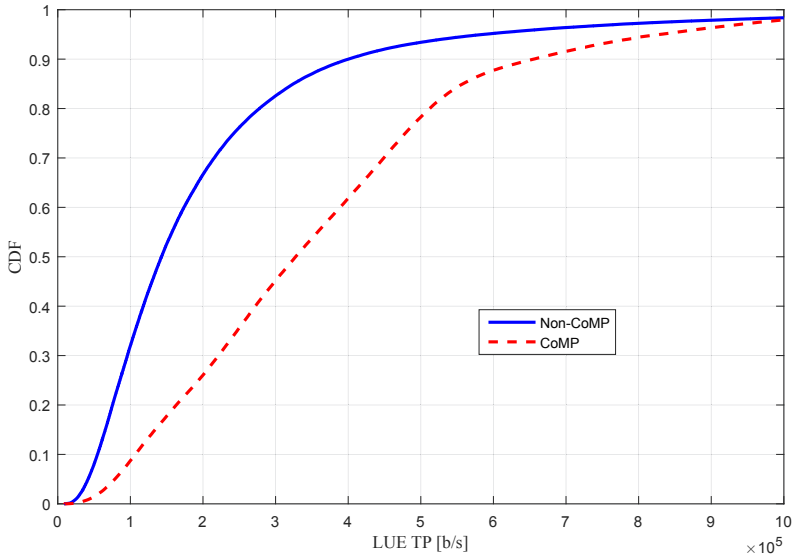

Figure 5.19. CDF for throughputs of LUEs for no CoMP and CoMP scenarios.

6. Conclusion

Inconsistent user experience caused by intercell interference is a key challenge in the contemporary and future mobile systems that reuse the whole assigned spectrum in every cell. The coordinated multipoint (CoMP) transmission has been studied to address the challenge through mitigating and/or exploiting the intercell interference, and the feature has been standardized by 3rd generation partnership project since long term evolution-advanced (LTE-A) Release 11. Literature has showed that different CoMP methods provide different performance gains and impose different implementation requirements.

In this thesis, we first introduced and analyzed the performance of hierarchically combined limited feedback techniques for CoMP. Although the hierarchical feedback structure might lead to suboptimal methods, it allows flexible combinations of different beamforming schemes with different implementation requirements. Analysis was carried out for a 2x2 transmit antenna system combining the so-called quantized cophasing (QCP) that applies quantized short-term channel phase feedback and the classical transmit selection combining. For the combined methods selection-QCP, QCP-selection, and QCP-QCP we derived in Section 3.3 verified analytical expressions for the expected signal-to-noise ratio (SNR), fading figure and average bit error rate (BER).

Performances of the combined methods are bounded by performance of the conventional antenna selection (lower bound) and the case where transmitter side employ full channel state information (upper bound). Performance improvement in terms of expected SNR and fading figure saturate soon when number of feedback bits used for QCP is increased: only negligible expected SNR and fading figure enhancements are obtained if we use more than 3-4 feedback bits. We also note that average BER results for QCP-QCP method when using only 3 and large number of

feedback bits for QCP overlap one another. Furthermore, we observe that the hierarchical QCP-QCP leads to negligible performance loss when compared to the non-hierarchical optimal joint co-phasing while the former method provides better implementation flexibility. Hence, results clearly point out that in addition to implementation flexibility very good performance can be reached by the hierarchical feedback structure.

This thesis work also studies the performance loss incurred in CoMP transmission due to channel power imbalance among coordinating points. The investigation has been done for the practical limited feedback methods QCP and ordered QCP (OQCP). In OQCP technique channel order statistics is applied at the transmitter side beside the channel phase information. For both QCP and OQCP, we derived closed-form expressions for the optimal amplitude weights, expected SNR, asymptotic capacity and BER assuming channel power imbalance. For benchmarking, we also recalled results for the conventional transmit selection combining and the case where full channel state information is applied at the transmitter side. Analytical results are presented in Section 4.4.

Even with few feedback bits and under channel power imbalance we observe that OQCP provides performance that is very close to the performance achieved with full channel state information. In terms of capacity and expected SNR, we see that QCP exploiting long-term signal amplitude information performs very close to OQCP. Thus, the use of amplitude feedback–fast or slow–is important in the presence of channel power imbalance. Furthermore, we note little performance difference between QCP and OQCP if number of diversity antennas in base stations is large. This is due to fact that fast signal variations becomes smaller when number of diversity antennas in base stations grows and fast selection of amplitude weights gives less gain over long term amplitude weights. Moreover, under power imbalance, we demonstrate that feedback error impacts the performance of OQCP more than it impacts the performance of the QCP, and the use of long-term amplitude weights for the QCP considerably decreases the performance loss resulting from the feedback errors.

Interestingly, unlike in the case of capacity and expected SNR, using SNR maximizing long-term amplitude weights for QCP may worsen the BER performance when base stations utilize single antenna for transmission due to limited diversity gain. This is not the case when base stations apply more than one diversity antennas.

The thesis also highlighted the use of self-backhauling for low power

nodes by exploiting the existing macro radio access network. This is a promising approach both in terms of cost-effectiveness of backhaul implementation and flexibility of low power node deployment. The backhaul capacity bottleneck which limit the low power node capacity was underlined as the primary limitation for the self-backhauling approach. To that end, we evaluated the use of QCP based joint transmission for relaxing the backhaul capacity bottleneck of self-backhauled LTE-A relays and LTE low power nodes in unlicensed band through extensive simulation campaign for exemplary LTE heterogeneous network deployments in a realistic urban scenarios.

Throughput results obtained from the simulation campaign assert that the CoMP significantly decreases the capacity gap between backhaul and access links. For instance, for the relay backhaul, the capacity gap is reduced by 86.00% at the 50%-ile when we allocate on backhaul 60% of the LTE subframes. This enhancement is accompanied by an approximately 80% low power node user equipment (UE) throughput gain at 50%-ile. Furthermore, we can use the CoMP gain at the backhaul to increase the performance of macro UEs so that throughput is improved not only for low power node UEs but also for macro UEs. We observe that CoMP with 30% backhaul subframes provides 26.38% throughput gain for all UEs at 50%-ile relative to the case of non-CoMP with 60% backhaul subframes. We note that CoMP also provides more even throughput distribution among UEs. Although these CoMP performance gains are sustained under feedback errors, it was also noted that considerable reduction in the gains are observed for large feedback bit error probability ($\geqslant 10\%$).

Besides, we formulated an analytical expression for the outage probability of the self-backhaul link assuming Rician channel towards donor base station and Rayleigh channel towards the remaining base stations. The respective results show that CoMP can considerably increase expected capacity for a certain outage probability.

As possible future works, we have suggested the following research items:

- Derive analytical expressions for different performance measures in case of hierarchical feedback structure with generalized MxN antennas. We expect that similar derivation approach used in this thesis can be used as a starting point for the analysis. Furthermore, the analysis can be extended for other relevant beamforming techniques.

- Extend the channel power imbalance analysis for more than two base stations. Furthermore, derivation of BER for any number of diversity antennas in base station and other modulation schemes are also worth considering.

- Evaluate further CoMP while relaxing backhaul capacity of low power nodes considering other semi-static or dynamic clustering methods and resource allocation approaches between backhaul and access links. Also other relevant CoMP methods and realistic deployment scenarios are important for future evaluations. The overall research question here is how to use CoMP efficiently and adaptively for the right low power node and at the right moment.

References

[1] Cisco, "Cisco visual networking index: global mobile data traffic forecast update, 2014-2019," white paper, Feb. 2015. [Online]. Available: http://www.cisco.com/

[2] H. Holma and A. Toskala, *LTE for UMTS - OFDMA and SC-FDMA Based Radio Access*. Chichester: Wiley, 2009.

[3] S. Parkvall, A. Furuskar, and E. Dahlman, "Evolution of LTE toward IMT-advanced," *IEEE Commun. Mag.*, vol. 49, no. 2, pp. 84–91, Feb. 2011.

[4] T. Wang, G. Li, J. Ding, Q. Miao, J. Li, and Y. Wang, "5G spectrum: is china ready?" *IEEE Commun. Mag.*, vol. 53, no. 7, pp. 58–65, Jul. 2015.

[5] V. Jungnickel, K. Manolakis, W. Zirwas, B. Panzner, V. Braun, M. Lossow, M. Sternad, R. Apelfrojd, and T. Svensson, "The role of small cells, coordinated multipoint, and massive MIMO in 5G," *IEEE Commun. Mag.*, vol. 52, no. 5, pp. 44–51, May 2014.

[6] A. Osseiran, F. Boccardi, V. Braun, K. Kusume, P. Marsch, M. Maternia, O. Queseth, M. Schellmann, H. Schotten, H. Taoka, H. Tullberg, M. Uusitalo, B. Timus, and M. Fallgren, "Scenarios for 5G mobile and wireless communications: the vision of the METIS project," *IEEE Commun. Mag.*, vol. 52, no. 5, pp. 26–35, May 2014.

[7] NGMN Alliance, "CoMP evaluation and enhancement," RAN Evolution Project deliverable, Mar. 2015.

[8] M. K. Karakayali, G. J. Foschini, and R. A. Valenzuela, "Network coordination for spectrally efficient communications in cellular systems," *IEEE Wireless Commun. Mag.*, vol. 13, no. 4, pp. 56–61, Aug. 2006.

[9] R. Irmer, H. Droste, P. Marsch, M. Grieger, G. Fettweis, S. Brueck, H. P. Mayer, L. Thiele, and V. Jungnickel, "Coordinated multipoint: Concepts, performance, and field trial results," *IEEE Commun. Mag.*, vol. 49, no. 2, pp. 102–111, Feb. 2011.

[10] X. Tao, X. Xu, and Q. Cui, "An overview of cooperative communications," *IEEE Commun. Mag.*, vol. 50, no. 6, pp. 65–71, Jun. 2012.

[11] H. Dahrouj and W. Yu, "Coordinated beamforming for the multicell multi-antenna wireless system," *IEEE Trans. Wireless Commun.*, vol. 9, no. 5, pp. 1748–1759, May 2010.

[12] J. Zhao, T. Quek, and Z. Lei, "Coordinated multipoint transmission with limited backhaul data transfer," *IEEE Trans. Wireless Commun.*, vol. 12, no. 6, pp. 2762–2775, Jun. 2013.

[13] 3GPP, "Coordinated multi-point operation for LTE physical layer aspects," 3GPP Technical Report, TR 36.819, Ver. 11.0.0, Sep. 2011.

[14] ——, "Coordinated multi-point operation for LTE with non-ideal backhaul," 3GPP Technical Report, TR 36.874, Ver. 12.0.0, Dec. 2013.

[15] M. Sawahashi, Y. Kishiyama, A. Morimoto, D. Nishikawa, and M. Tanno, "Coordinated multipoint transmission/reception techniques for LTE-advanced," *IEEE Wireless Commun. Mag.*, vol. 17, no. 3, pp. 26–34, Jun. 2010.

[16] Z. Bai, S. Iwelski, G. Bruck, P. Jung, B. Badic, T. Scholand, and R. Balraj, "Evaluation of implicit feedback in coordinated multipoint transmission beyond LTE-Advanced," in *Proc. IEEE Veh. Tech. Conf. Spring*, Jun. 2013, pp. 1–5.

[17] V. Kotzsch and G. Fettweis, "On synchronization requirements and performance limitations for CoMP systems in large cells," in *8th International Workshop on Multi-Carrier Systems Solutions (MC-SS)*, May 2011, pp. 1–5.

[18] S. Sun, Q. Gao, Y. Peng, Y. Wang, and L. Song, "Interference management through CoMP in 3GPP LTE-advanced networks," *IEEE Trans. Wireless Commun.*, vol. 20, no. 1, pp. 59–66, Feb. 2013.

[19] Y. Zhou, L. Liu, H. Du, L. Tian, X. Wang, and J. Shi, "An overview on inter-cell interference management in mobile cellular networks: From 2G to 5G," in *Proc. IEEE Int. Conf. on Commun.*, Nov. 2014, pp. 217–221.

[20] Y. Wang, W. Feng, L. Xiao, Y. Zhao, and S. Zhou, "Coordinated multi-cell transmission for distributed antenna systems with partial CSIT," *IEEE Commun. Lett.*, vol. 16, no. 7, pp. 1044–1047, Jul. 2012.

[21] L. Venturino, N. Prasad, and X. Wang, "Coordinated scheduling and power allocation in downlink multicell OFDMA networks," *IEEE Trans. Veh. Technol.*, vol. 58, no. 6, pp. 2835–2848, Jul. 2009.

[22] H. Zhang, L. Venturino, N. Prasad, P. Li, S. Rangarajan, and X. Wang, "Weighted sum-rate maximization in multi-cell networks via coordinated scheduling and discrete power control," *IEEE Journal Selected Areas in Communications*, vol. 29, no. 6, pp. 1214–1224, Jun. 2011.

[23] D. Love, R. Heath, V. Lau, D. Gesbert, B. Rao, and M. Andrews, "An overview of limited feedback in wireless communication systems," *IEEE Journal Selected Areas in Communications*, vol. 26, no. 8, pp. 1341–1365, Oct. 2008.

[24] R. W. Heath (Jr.) and A. Paulraj, "A simple scheme for transmit diversity using partial channel feedback," in *Proc. Asilomar Conf. on Signals, Systems and Computers*, vol. 2, Nov. 1998, pp. 1073–1078.

[25] J. C. Roh and B. D. Rao, "Transmit beamforming in multiple-antenna systems with finite rate feedback: A VQ-based approach," *IEEE Trans. Inf. Theory*, vol. 52, no. 3, pp. 1101–1112, Mar. 2006.

[26] R.-A. Pitaval, H.-L. Maattanen, K. Schober, O. Tirkkonen, and R. Wichman, "Beamforming codebooks for two transmit antenna systems based on optimum grassmannian packings," *IEEE Trans. Inf. Theory*, vol. 57, no. 10, pp. 6591–6602, Oct. 2011.

[27] 3GPP, "Further advancements for E-UTRA physical layer aspects," 3GPP Technical Specification, TR 36.814, Ver. 9.0.0, Mar. 2010.

[28] ——, "Coordinated multi-point operation for LTE physical layer aspects," 3GPP Technical Report, TR 36.819, Ver. 11.2.0, Sep. 2013.

[29] Q. Cui, H. Wang, P. Hu, X. Tao, P. Zhang, J. Hamalainen, and L. Xia, "Evolution of limited-feedback CoMP systems from 4G to 5G: CoMP features and limited-feedback approaches," *IEEE Veh. Technol. Mag.*, vol. 9, no. 3, pp. 94–103, Sep. 2014.

[30] J. Hämäläinen and R. Wichman, "Performance analysis of closed-loop transmit diversity in the presence of feedback errors," in *Proc. IEEE Int. Symp. on Personal, Indoor and Mobile Radio Commun.*, vol. 5, Sep. 2002, pp. 2297–2301.

[31] T. Ramya and S. Bhashyam, "Using delayed feedback for antenna selection in MIMO systems," *IEEE Trans. Wireless Commun.*, vol. 8, no. 12, pp. 6059–6067, Dec. 2009.

[32] A. Heidari and A. Khandani, "Closed-loop transmit diversity with imperfect feedback," *IEEE Trans. Wireless Commun.*, vol. 9, no. 9, pp. 2737–2741, Sep. 2010.

[33] M. Duarte, A. Sabharwal, C. Dick, and R. Rao, "Beamforming in MISO systems: Empirical results and EVM-Based analysis," *IEEE Trans. Wireless Commun.*, vol. 9, no. 10, pp. 3214–3225, Oct. 2010.

[34] D. Jaramillo-Ramirez, M. Kountouris, and E. Hardouin, "Coordinated multi-point transmission with quantized and delayed feedback," in *Proc. IEEE Global Telecommun. Conf.*, Dec. 2012, pp. 2391–2396.

[35] T. Biermann, L. Scalia, C. Choi, W. Kellerer, and H. Karl, "How backhaul networks influence the feasibility of coordinated multipoint in cellular networks," *IEEE Commun. Mag.*, vol. 51, no. 8, pp. 168–176, August 2013.

[36] V. Pichapati and P. Gupta, "Practical considerations in cluster design for coordinated multipoint (comp) systems," in *Proc. IEEE Int. Conf. on Commun.*, Jun. 2013, pp. 5860–5865.

[37] Y. Beyene, R. Jantti, and K. Ruttik, "Cloud-RAN Architecture for Indoor DAS," *IEEE Access*, vol. 2, pp. 1205–1212, Oct. 2014.

[38] A. Narula, M. J. Lopez, M. D. Trott, and G. W. Wornell, "Efficient use of side information in multiple-antenna data transmission over fading channels," *IEEE Journal Selected Areas in Communications*, vol. 16, no. 8, pp. 1423–1436, Oct. 1998.

[39] J. Hämäläinen and R. Wichman, "Asymptotic bit error probabilities of some closed-loop transmit diversity schemes," in *Proc. IEEE Global Telecommun. Conf.*, vol. 1, Nov. 2002, pp. 360–364.

[40] J. Hämäläinen, R. Wichman, A. A. Dowhuszko, and G. Corral-Briones, "Capacity of generalized UTRA FDD closed-loop transmit diversity modes," *Wireless Personal Communications*, pp. 1–18, May 2009.

[41] J. Hämäläinen and R. Wichman, "On the performance of FDD WCDMA closed-loop transmit diversity modes in Nakagami and Ricean fading channels," in *Proc. IEEE Int. Symp. on Spread Spectrum Techniques and Applications*, vol. 1, Sep. 2002, pp. 24–28.

[42] 3GPP, "Physical layer procedures (FDD)," 3GPP Technical Specification, TS 25.214, Ver. 13.0.0, Sep. 2013.

[43] ——, "Physical channels and modulation," 3GPP Technical Specification, TS 36.211, Ver. 12.7.0, Sep. 2015.

[44] J. Hämäläinen and R. Wichman, "Closed-loop transmit diversity for FDD WCDMA systems," in *Proc. Asilomar Conf. on Signals, Systems and Computers*, vol. 1, Oct. 2000, pp. 111–115.

[45] 3GPP, "Physical layer procedures (FDD)," 3GPP Technical Specification, TS 25.214, Ver. 4.6.0, Apr. 2003.

[46] M. K. Simon and M.-S. Alouini, *Digital Communication Over Fading Channels*. John Wiley and Sons, 2005.

[47] A. Goldsmith, *Wireless Communications*. Cambridge University Press, 2005.

[48] P. Mogensen, W. Na, I. Kovacs, F. Frederiksen, A. Pokhariyal, K. Pedersen, T. Kolding, K. Hugl, and M. Kuusela, "LTE capacity compared to the Shannon bound," in *Proc. IEEE Veh. Tech. Conf. Spring*, Apr. 2007, pp. 1234–1238.

[49] E. Lahetkangas, K. Pajukoski, E. Tiirola, J. Hamalainen, and Z. Zheng, "On the performance of LTE-Advanced MIMO: How to set and reach beyond 4G targets," in *18th European Wireless Conference*, Apr. 2012, pp. 1–6.

[50] M. Abramowitz and I. A. Stegun, *Handbook of Mathematical Functions: with Formulas, Graphs, and Mathematical Tables*. Dover Publications, 1972.

[51] A. Haghighat, "UE calibration in MIMO systems," in *Proc. IEEE Veh. Tech. Conf. Spring*, Sept 2012, pp. 1–4.

[52] A. Saleh, A. Rustako, and R. Roman, "Distributed antennas for indoor radio communications," *IEEE Trans. Commun.*, vol. 35, no. 12, pp. 1245–1251, Dec. 1987.

[53] L. Xiao, L. Dai, H. Zhuang, S. Zhou, and Y. Yao, "Information-theoretic capacity analysis in MIMO distributed antenna systems," in *Proc. IEEE Veh. Tech. Conf. Spring*, vol. 1, Apr. 2003, pp. 779–782.

[54] E. Song, J. Park, J. Kim, S. Hwang, and W. Sung, "Performance of cooperative transmission schemes using distributed antennas," in *Proc. IEEE Consum. Commun. and Networking Conf.*, Jan. 2008, pp. 41–45.

[55] H. C. Papadopoulos and C.-E. W. Sundberg, "Space-time codes for MIMO systems with non-collocated transmit antennas," *IEEE Journal Selected Areas in Communications*, vol. 26, no. 6, pp. 927–937, Aug. 2008.

[56] J. H. Winters, "On the capacity of radio communication systems with diversity in a rayleigh fading environment," *IEEE Journal Selected Areas in Communications*, vol. 5, no. 5, pp. 871–878, Jun. 1987.

[57] G. J. Foschini and M. J. Gans, "On limits of wireless communications in a fading environment when using multiple antennas," *Wireless Personal Commun.*, vol. 6, no. 3, pp. 311–335, Mar. 1998.

[58] 3GPP, "E-UTRA lte physical layer," 3GPP Technical Specification, TR 36.874, Ver. 12.2.0, Mar. 2015.

[59] M.-S. Alouini and A. J. Goldsmith, "Capacity of Rayleigh fading channels under different adaptive transmission and diversity-combining techniques," *IEEE Trans. Veh. Technol.*, vol. 48, no. 4, pp. 1165–1181, Jul. 1999.

[60] A. Coskun and O. Kucur, "Performance analysis of joint single transmit and receive antenna selection in non-identical nakagami-m fading channels," *IET Communications,*, vol. 5, no. 14, pp. 1947–1953, Sep. 2011.

[61] J. Romero-Jerez and A. Goldsmith, "Performance of multichannel reception with transmit antenna selection in arbitrarily distributed nagakami fading channels," *IEEE Trans. Wireless Commun.*, vol. 8, no. 4, pp. 2006–2013, Apr. 2009.

[62] J. Hamalainen and R. Wichman, "Asymptotic bit error probabilities of some closed-loop transmit diversity schemes," in *Proc. IEEE Global Telecommun. Conf.*, vol. 1, 17-21 2002, pp. 360–364 vol.1.

[63] Winprop software package. [Online]. Available: http://www.awe-communications.com/

[64] Y.-D. Yao and A. Sheikh, "Outage probability analysis for microcell mobile radio systems with cochannel interferers in Rician/Rayleigh fading environment," *Electronics Letters*, vol. 26, no. 13, pp. 864–866, June 1990.

[65] O. Eluwole and M. Lohi, "Coordinated multipoint power consumption modeling for energy efficiency assessment in LTE/LTE-advanced cellular networks," in *19th International Conference on Telecommunications (ICT)*, April 2012, pp. 1–6.

[66] FP7 METIS, "Scenarios, requirements and KPIs for 5G mobile and wireless system," Project deliverable D1.1, Apr. 2014.

[67] T. Sakano, Z. Fadlullah, T. Ngo, H. Nishiyama, M. Nakazawa, F. Adachi, N. Kato, A. Takahara, T. Kumagai, H. Kasahara, and S. Kurihara, "Disaster-resilient networking: a new vision based on movable and deployable resource units," *IEEE Netw.*, vol. 27, no. 4, pp. 40–46, Jul. 2013.

[68] J. Robson, "Small cell deployment strategies and best practice backhaul," Cambridge broadband networks, white paper, Aug. 2012.

[69] P. Blasco, M. Bennis, and M. Dohler, "Backhaul-aware self-organizing operator-shared small cell networks," in *Proc. IEEE Int. Conf. on Commun.*, Jun. 2013, pp. 2801–2806.

[70] C. Hoymann, W. Chen, J. Montojo, A. Golitschek, C. Koutsimanis, and X. Shen, "Relaying operation in 3GPP LTE: challenges and solutions," *IEEE Commun. Mag.*, vol. 50, no. 2, pp. 156–162, Feb. 2012.

[71] Qualcomm, "Rising to meet the 1000x mobile data challenge," white paper, 2012. [Online]. Available: http://www.qualcomm.com/media/documents/

[72] Z. Roth, M. Goldhamer, N. Chayat, A. Burr, M. Dohler, N. Bartzoudis, C. Walker, Y. Leibe, C. Oestges, M. Brzozowy, and I. Bucaille, "Vision and architecture supporting wireless GBit/sec/km^2 capacity density deployments," in *Future Network and Mobile Summit*, Jun. 2010.

[73] IEEE, "Architecture and requirements for small cell backhaul," IEEE 802.16r, Tech. Rep., 2013.

[74] O. Bulakci, S. Redana, B. Raaf, and J. Hamalainen, "Performance enhancement in LTE-Advanced relay networks via relay site planning," in *Proc. IEEE Veh. Tech. Conf. Spring*, May 2010, pp. 1–5.

[75] O. Bulakci, A. Bou Saleh, J. Hamalainen, and S. Redana, "Performance analysis of relay site planning over composite fading/shadowing channels with cochannel interference," *IEEE Trans. Veh. Technol.*, vol. 62, no. 4, pp. 1692–1706, May 2013.

[76] A. Saleh, O. Bulakci, J. Hämäläinen, S. Redana, and B. Raaf, "Analysis of the impact of site planning on the performance of relay deployments," *IEEE Trans. Veh. Technol.*, vol. 61, no. 7, pp. 3139–3150, Sept 2012.

[77] I. Maric, B. Bostjancic, and A. Goldsmith, "Resource allocation for constrained backhaul in picocell networks," in *Information Theory and Applications Workshop*, Feb. 2011, pp. 1–6.

[78] A. Coluccia, A. D'Alconzo, and F. Ricciato, "On the optimality of max-min fairness in resource allocation." *Annales of Telecommunications*, vol. 67, no. 1-2, pp. 15–26, 2012.

[79] R. Jain, D. Chiu, and W. Hawe, "A quantitative measure of fairness and discrimintation for resource allocation in shared computer systems," Digital Equipment Corporation Technical Report, TR 301, Sep. 1984.

[80] J. Andrews, "Seven ways that HetNets are a cellular paradigm shift," *IEEE Commun. Mag.*, vol. 51, no. 3, pp. 136–144, Mar. 2013.

[81] Ericsson, "LTE licensed assited access," Presentation, Jan. 2015. [Online]. Available: http://www.ericsson.com/

[82] Qualcomm, "Extending LTE Advanced towards unlicensed spectrum," white paper, Dec. 2013. [Online]. Available: https://www.qualcomm.com/documents/

[83] F. Abinader, E. Almeida, F. Chaves, A. Cavalcante, R. Vieira, R. Paiva, A. Sobrinho, S. Choudhury, E. Tuomaala, K. Doppler, and V. Sousa, "Enabling the coexistence of LTE and Wi-Fi in unlicensed bands," *IEEE Commun. Mag.*, vol. 52, no. 11, pp. 54–61, Nov. 2014.

[84] Opencellid. [Online]. Available: http://opencellid.org/

[85] 3GPP, “Small cell enhancements for E-UTRA and E-UTRAN-Physical layer aspects,” 3GPP Technical Report, TR 36.872, Ver. 12.1.0, Dec. 2013.

Errata

Publication I

The ’ss’ in equation (9) should be ’fi’.

Publication IV

The phrase ’greater than’ in Paragraph 1 of Section IV should be replaced with ’less than’.

In mobile systems there is a need to guarantee homogeneous quality of experience (QoE) independent of user location in the network. However, the presence of intercell interference (ICI) is the primary cause of inconsistent QoE, especially for users located on the cell edge. The effects of ICI are further exacerbated with increasing density of base stations. Therefore, in densely deployed mobile systems coordinated transmission methods are critical for guaranteeing acceptable user QoE through mitigation of ICI. The main motivation of this research is to study the performance enhancements enabled by the effective implementation of practically feasible CoMP transmission. To achieve the aforementioned goal, this dissertation proposes and analyzes practical methods for the effective realization of CoMP transmission and contributes to new knowledge on the limits of CoMP transmission performance gains for realistic implementations and deployment scenarios.

Aalto-DD 129/2016

ISBN 978-952-60-6895-4 (printed)
ISBN 978-952-60-6896-1 (pdf)
ISSN-L 1799-4934
ISSN 1799-4934 (printed)
ISSN 1799-4942 (pdf)

Aalto University

Department of Communications and Networking
www.aalto.fi

BUSINESS + ECONOMY

ART + DESIGN + ARCHITECTURE

SCIENCE + TECHNOLOGY

CROSSOVER

DOCTORAL DISSERTATIONS